Srs2 binding to PCNA and its sumoylation contribute to RPA antagonism during the DNA damage response

Jiayi Fan[1], Nalini Dhingra[1#], Tammy Yang[2], Vicki Yang[2], Xiaolan Zhao[1]

[1]Molecular Biology Program, Memorial Sloan Kettering Cancer Center, New York, NY 10065

[2]City University of New York Hunter College, New York, NY 10065

Current address: Yale Center for Molecular Discovery, Yale University, West Haven, CT 06516

Corresponding author email: zhaox1@mskcc.org

Key words: DNA damage checkpoint, checkpoint dampening, Srs2, RPA, sumoylation, PCNA

Abstract

Activation of the DNA damage checkpoint upon genotoxin treatment induces a multitude of cellular changes to cope with genome stress. After prolonged genotoxin treatment, the checkpoint can be downregulated to allow cell cycle and growth resumption. In yeast, downregulation of the DNA damage checkpoint requires the Srs2 DNA helicase, which removes the ssDNA binding complex RPA and the associated Mec1 checkpoint kinase from DNA, thus dampening Mec1-mediated checkpoint. However, it is unclear whether the 'anti-checkpoint' role of Srs2 is temporally and spatially regulated to allow timely checkpoint termination while preventing superfluous RPA removal. Here we address this question by examining regulatory elements of Srs2, such as its phosphorylation, sumoylation, and protein-interaction sites. Our genetic analyses and checkpoint level assessment suggest that the RPA countering role of Srs2 is promoted by Srs2 binding to PCNA, which recruits Srs2 to a subset of ssDNA containing regions. RPA antagonism is further fostered by Srs2 sumoylation, which we found depending on the Srs2-PCNA interaction and Mec1, and peaking after Mec1 activity reaches maximal levels. These data suggest that Srs2 recruitment to PCNA proximal ssDNA-RPA filaments followed by its sumoylation can promote checkpoint recovery, whereas Srs2 action is minimized at regions with no proximal PCNA to permit RPA-mediated ssDNA protection.

Introduction

The DNA damage response promotes organismal survival of genotoxic stress by eliciting many cellular changes. A critical component of this response is a signaling process termed the DNA damage checkpoint (DDC) (Enoch *et al.*, 1992, Hartwell and Weinert, 1989, Lanz *et al.*, 2019). Upon experiencing genotoxic stress, apical DDC kinases are recruited to DNA lesion sites by the damage sensing proteins and are then activated by activator proteins (Usui *et al.*, 2001, Zou and Elledge, 2003). A universal DDC sensor is the RPA complex that binds with high affinity and specificity to single-strand DNA (ssDNA), whose abundance rises under almost all types of genotoxic stress (Marechal and Zou, 2015). Using the budding yeast system as an example, RPA bound to the ssDNA filament can interact with Ddc2 (homolog of the human ATRIP protein), the co-factor of the Mec1 (homolog of the human ATR protein) checkpoint kinase, and recruit the Mec1-Ddc2 complex to DNA lesion sites (Elledge, 1996, Foiani *et al.*, 2000). Subsequently, Mec1 is activated by activator proteins, such as the 9-1-1 complex loaded at the 5' DNA ends at ssDNA and double strand (ds) DNA junctions. Activated Mec1 can then phosphorylate multiple substrates, among which is a key downstream effector kinase Rad53, the phosphorylation of which turns on its own kinase activity and yields further phosphorylation events (Harrison and Haber, 2006). Collectively, the DDC kinases can modify hundreds of proteins, inducing multitude of pathway changes (Lanz *et al.*, 2019). For example, DDC can arrest or delay the cell cycle progression to allow more time for genome repair (Sanchez *et al.*, 1999, Wang *et al.*, 2001).

While DDC activation is crucial for the cell to cope with genotoxic stress, its timely downregulation is equally vital (Waterman *et al.*, 2020). Many changes induced by the DDC kinases need to be reversed to allow continued cell growth and recovery. For example, the DDC-mediated cell cycle arrest has to be lifted to allow proliferation and alternative DNA repair mechanisms permitted at other cell cycle phases (Pellicioli *et al.*, 2001, Waterman *et al.*, 2020). Thus far, DDC downregulation has been mainly studied using the model organism yeast, with several strategies being identified (Waterman *et al.*, 2020). One of these is mediated by the DNA helicase Srs2 that targets the most upstream step of the DDC pathway through removing RPA and the associated Mec1-Ddc2 from chromatin (Dhingra *et al.*, 2021). Importantly, the role of Srs2 in DDC dampening (anti-checkpoint) can be separated from its well-studied role in removing the recombinase Rad51 from ssDNA (anti-recombination) that modulates homologous recombination levels and outcomes (Dhingra *et al.*, 2021). The former role of Srs2 is critical for cell survival of genotoxins, such as camptothecin (CPT) that traps Top1 on DNA (Dhingra *et al.*, 2021). Considering that other organisms also possess DNA helicases capable of removing RPA from ssDNA (Hormeno *et al.*, 2022, Jenkins *et al.*, 2021, Shorrocks *et al.*, 2021), it is plausible that an anti-checkpoint strategy involving RPA antagonism may be present beyond yeast.

Currently, little is known about how checkpoint dampening can be temporally controlled to minimize interference with the initial DDC activation that must occur in the early phase of the DNA damage response. In the case of the Srs2-mediated checkpoint regulation, it is also unclear how the process can minimize superfluous removal of RPA from ssDNA sites that unlikely induce the DDC due to lacking 5' DNA ends at ss-dsDNA junctions for 9-1-1 loading, such as at those formed at R-loops. The main functions of RPA at these sites can be ssDNA protection and repair, rather than DDC induction, thus these sites may benefit from shielding from Srs2-mediated RPA removal. In addressing these questions, we hypothesize that Srs2-based RPA antagonism should be selective in location and timing, and that the regulatory elements within the Srs2 protein may contribute to such selectivity.

To examine the above hypothesis and to define Srs2 features relevant to its RPA antagonism during DDC regulation, we inspected Srs2 protein sites involved in its post-translational modifications and interactions with other proteins. Our genetic analyses of mutations affecting each of these sites suggest that while most of the examined features do not affect RPA antagonism, Srs2 binding to PCNA, which marks 3' DNA ends of ss-dsDNA junctions that flank ssDNA gaps or tails, and Srs2 sumoylation contribute to RPA regulation in the context of DDC. Srs2 binding to PCNA is known to recruit Srs2 to replication perturbation sites, while the roles of Srs2 sumoylation were less clear (Kolesar *et al.*, 2012, Moldovan *et al.*, 2007, Papouli *et al.*, 2005, Pfander *et al.*, 2005, Saponaro *et al.*, 2010). Unexpectedly, we found that Srs2 binding to PCNA and Srs2 sumoylation are functionally related, since PCNA binding promotes Srs2 sumoylation. Moreover, Srs2 sumoylation level peaks late in the response to genomic stress after the DDC kinases are hyper-activated, and this modification depends on the Mec1 checkpoint kinase. Collectively, our data suggest a model wherein Srs2 can distinguish between two types of ssDNA regions using PCNA proximity as a guide for subsequent sumoylation, RPA removal, and countering hyper-activated checkpoint.

Results

Srs2 regulatory features and their disabling mutants

To understand which Srs2 attributes are relevant to RPA regulation during the DNA damage response, we examined mutant alleles that perturb known features of the Srs2 protein. Srs2 was reported to contain a helicase domain at its N-terminal region and three protein-protein interaction sites at its C-terminal region (Fig. 1A) (Niu and Klein, 2017). We have previously shown that the Srs2 ATPase-dead allele (*srs2-K41A*) fails to downregulate both RPA levels on chromatin and the Mec1-mediated DDC, indicating a requirement of ATPase-driven stripping of RPA from ssDNA (Dhingra *et al.*, 2021). The reported Srs2 protein-bindings sites include a Rad51 binding domain (Rad51-BD), a PCNA interaction motif (PIM), and a SUMO interaction motif (SIM) (Fig. 1A) (Armstrong *et al.*, 2012, Colavito *et al.*, 2009, Kolesar *et al.*, 2016, Kolesar *et al.*, 2012, Papouli *et al.*, 2005). We employed CRISPR-based editing to generate the *srs2-Δ*PIM* (Δ1159-1163 amino acids) and the *srs2-SIM*^{mut} ($_{1170}$IIVID$_{1174}$ to $_{1170}$AAAAD$_{1174}$) alleles used in previous studies and examined an established *srs2-Δ*Rad51BD* allele (Δ875-902 amino acids) (Armstrong *et al.*, 2012, Colavito *et al.*, 2009, Kolesar *et al.*, 2016, Kolesar *et al.*, 2012, Papouli *et al.*, 2005). We note that despite Srs2 can remove of RPA from ssDNA, an interaction between the two proteins has yet to be reported.

We also queried post-translational modifications reported for Srs2 by mutating the corresponding modification sites (Fig. 1A). First, seven Cdk1 phosphorylation consensus sites of Srs2 were mutated to produce the *srs2-7AV* (T604V, S698A, S879A, S893A, S938A, S950A, and S965A) allele (Chiolo *et al.*, 2005), which was previously shown to affect homologous recombination. Second, three sumoylation sites of Srs2 were mutated to generate *srs2-3KR* (K1081R, K1089R, and K1142R) (Saponaro *et al.*, 2010). Finally, we mutated two serine residues (S890 and S933) to alanine to generate *srs2-2SA*, since phosphorylation at these sites was identified in proteomic studies as dependent on both the Mec1 kinase and genotoxic treatments (Faca *et al.*, 2020). Because the Srs2 C-terminal end contributes to the protein's functions (Antony *et al.*, 2009, Colavito *et al.*, 2009), the six mutant alleles described above were not tagged with epitopes at its C-terminus. Using an anti-Srs2 specific antibody, we showed that all six alleles supported wild-type levels of Srs2 protein based on immunoblotting (Fig. 1B).

149
150 **Mutating PCNA binding and sumoylation sites of Srs2 rescues *rfa1-zm2* CPT sensitivity**
151
152 Srs2 loss leads to persistent DDC and perturbed recombination, both of which contribute to
153 *srs2*Δ sensitivity to genotoxins, including CPT and methyl methanesulfonate (MMS) (Fig. 2A)
154 (Niu and Klein, 2017). Significantly, our recent study has shown that RPA mutants that reduce
155 its ssDNA binding affinity rescue the persistent DDC levels in *srs2*Δ cells but not their
156 recombination defects (Dhingra *et al.*, 2021). *rfa1-zm2* (N492D, K493R, K494R) is one of the
157 RPA alleles examined that contains mutations at three DNA contacting residues in the Rfa1
158 subunit of RPA (Fan and Pavletich, 2012). Purified RPA complex containing these mutations
159 exhibited a two-fold increase in dissociation constant using ssDNA as substrate, compared to
160 the wild-type RPA complex (Dhingra *et al.*, 2021). In cells, *rfa1-zm2* supports normal Rfa1
161 protein level, cell growth, DNA replication (Dhingra *et al.*, 2021). It also did not affect gene
162 conversion, direct repeat repair or rDNA recombination, nor the hyper-recombination phenotype
163 of *srs2*Δ (Dhingra *et al.*, 2021). However, *rfa1-zm2* and *srs2*Δ are mutually suppressive for both
164 their genotoxic sensitivities and their DDC abnormalities (Fig. 2B, S1A) (Dhingra *et al.*, 2021).
165 These data suggest that the *srs2* and *rfa1-zm2* genetic relationship can be used as a readout
166 for the antagonism between Srs2 and RPA in DDC and that this functional relationship can be
167 separable for Srs2's anti-recombination role stemming from Rad51 regulation. Based on this
168 rationale, we employed the genetic suppression as an initial readout in querying whether any of
169 the six *srs2* mutant alleles described above are related to RPA regulation. Given that Srs2's role
170 in checkpoint dampening was best examined in CPT (Dhingra *et al.*, 2021), which induces the
171 DNA damage checkpoint to delay G2/M progression, but does not induce the DNA replication
172 checkpoint, experiments were mostly carried out in this condition.
173
174 We found that on their own, *srs2-ΔPIM*, *SIM*^{mut}, and *-7AV* showed different levels of
175 sensitivity toward CPT at a concentration ranging from 2 to 8 μg/ml, while *srs2-ΔRad51BD* and -
176 *3KR* exhibited close to wild-type level of CPT resistance, which are consistent with previous
177 reports (Colavito *et al.*, 2009, Saponaro *et al.*, 2010) (Fig. S1A). In addition, *srs2-2SA,* which
178 has not been examined previously*,* did not show CPT sensitivity (Fig. S1A). Since *rfa1-zm2*
179 cells exhibited stronger CPT sensitivity than the tested *srs2* alleles (Fig. S1A), we asked if the
180 latter could suppress *rfa1-zm2* CPT sensitivity. We found that both *srs2-ΔPIM* and *-3KR*
181 improved the CPT resistance of *rfa1-zm2* cells on media containing 2 μg/ml CPT (Fig. 2C).
182 Rescue was also seen at higher CPT concentrations, with *srs2-ΔPIM* exhibiting a stronger effect
183 than *srs2-3KR* (Fig. S1B). In contrast to *srs2-ΔPIM* and *srs2-3KR*, *srs2-ΔRad51BD* and *-2SA*
184 showed no effect on *rfa1-zm2* growth on media containing CPT, whereas *srs2*-7AV *and -SIM*^{mut}
185 worsened it (Fig. 2D). The differential effects seen for the *srs2* alleles are consistent with the
186 notion that Srs2 has multiple roles in cellular survival of genotoxic stress (Bronstein *et al.*, 2018,
187 Niu and Klein, 2017). The unique suppression seen for mutants affecting Srs2 binding to PCNA
188 and its sumoylation suggests that these features are relevant to RPA regulation during the DNA
189 damage response.
190
191
192 **Additional suppressive effects conferred by *srs2-ΔPIM* and *-3KR* toward *rfa1* mutants**
193
194 We next tested whether the observed *srs2-ΔPIM* and *-3KR* suppression was specific towards
195 *rfa1-zm2* or applicable to other *rfa1* mutants that are also defective in ssDNA binding. While
196 *rfa1-zm2* affects the ssDNA binding domain C (DBD-C) of Rfa1, a widely used *rfa1* allele, *rfa1-*
197 *t33,* impairs the DBD-B domain (Fig. 2E) (Umezu *et al.*, 1998). Unlike *rfa1-zm2, rfa1-t33*
198 additionally decreases Rfa1 protein level and interferes with DNA replication and repair (Deng *et*
199 *al.*, 2014, Umezu *et al.*, 1998). Despite having these additional defects, CPT survival of *rfa1-t33*

200 cells was also improved by *srs2-ΔPIM* or *srs2-3KR* (Fig. 2E). As seen in the case of *rfa1-zm2*,
201 *srs2-ΔPIM* conferred better rescue than *srs2-3KR* toward *rfa1-t33* (Fig. 2E). When comparing
202 the two *rfa1* alleles, *srs2* rescue was stronger toward *rfa1-zm2*, likely because *rfa1-t33* has
203 other defects besides reduced ssDNA binding (Fig. 2C, 2E). In either case, *srs2* mutants only
204 conferred partial suppression, consistent with the notion that Srs2 has roles beyond RPA
205 regulation, such as in Rad51 regulation and removing DNA joint molecules (Bronstein *et al.*,
206 2018, Niu and Klein, 2017). Nevertheless, the observed rescue of both *rfa1-zm2* and *rfa1-t33*
207 provided strong genetic evidence that Srs2 binding to PCNA and sumoylation are involved the
208 regulation of RPA during the DNA damage response.
209
210 Srs2 regulation of RPA during DDC is not only observed under CPT treatment, but is
211 also seen in treatment with MMS (Dhingra *et al.*, 2021), which induces both DDS and the DNA
212 replication checkpoint and thus delaying both S phase progression and G2/M phase exit
213 (Paciotti *et al.*, 2000, Tercero *et al.*, 2003). Consistent with observation made in CPT conditions,
214 *srs2-ΔPIM* moderately improved the MMS sensitivity of *rfa1-zm2* and *rfa1-t33,* while *srs2-3KR*
215 had a small effect on the MMS sensitivity of *rfa1-zm2* (Fig. S1B, S1C). The degrees of
216 suppression seen in MMS treatment were less than those observed in CPT conditions, and we
217 address likely reasons for this difference in Discussion. Collectively, the multiple genetic results
218 are consistent among themselves and provide evidence that the roles of Srs2 binding to PCNA
219 and sumoylation in RPA antagonism can be applicable to more than one genomic stress
220 situation.
221
222
223 ***srs2-ΔPIM* and *-3KR* rescue checkpoint abnormality of *rfa1-zm2* cells**
224
225 We next investigated whether *srs2-ΔPIM* and *-3KR* suppression of the DNA damage sensitivity
226 of *rfa1-zm2* cells pertained to DDC regulation. We employed two readouts for DDC that are
227 widely used. First, we used the F9 antibody, which specifically recognizes phosphorylated
228 Rad53, to measure the levels of activated Rad53 (Fiorani *et al.*, 2008). Second, we measure
229 cellular ability to timely exit the G2/M phase after CPT treatment using FACS analyses. We note
230 that CPT-induced DDC leads to G2/M delay rather than an arrest as shown in previous studies
231 (Dhingra *et al.*, 2021, Menin *et al.*, 2018, Redon *et al.*, 2003). We recently reported that *srs2Δ*
232 cells exhibit increased levels of phosphorylated Rad53 and diminished ability to timely exit G2/M
233 phase in CPT, and that both are suppressed by *rfa1-zm2* (Dhingra *et al.*, 2021). Interestingly,
234 *rfa1-zm2* leads to similar defects and these are rescued by *srs2Δ* (Dhingra *et al.*, 2021) (Fig.
235 3A). The mutual suppression seen in these assays is consistent with that seen for CPT
236 sensitivity (Dhingra *et al.*, 2021). We note that several other RPA ssDNA binding mutants, such
237 as *rfa1-t33*, also exhibit phenotypes indicative of increased DDC levels (Pellicioli *et al.*, 2001,
238 Seeber *et al.*, 2016, Smith and Rothstein, 1995, Zou and Elledge, 2003). This is likely because
239 compromised ssDNA protection can lead to increased levels of DNA lesions thus enhancing the
240 activation of Mec1 and/or its homolog Tel1.
241
242 We reasoned that if *srs2-ΔPIM* and *srs2-3KR* compromise Srs2's ability to remove RPA
243 from DNA in cells, they should alleviate *rfa1-zm2* cells' defects in ssDNA protection and the
244 associated DDC abnormalities (Fig. 3A). Indeed, while *rfa1-zm2* exhibited about 5-fold increase
245 in Rad53 phosphorylation levels in CPT compared with wild-type cells as seen before (Dhingra
246 *et al.*, 2021), *srs2-ΔPIM* and *-3KR* reduced this level by about 50% and 80%, respectively (Fig.
247 3B). Similar to earlier data, we observed that wild-type cells arrested in G_2/M after 1 hour of CPT
248 treatment and about 25% of these cells entered G_1 after another hour (Fig. 3C) (Dhingra *et al.*,
249 2021). The ability to timely exit from G_2/M was reduced in *rfa1-zm2* cells so that only 13% cells
250 moved to G1 after 2 h treatment with CPT, as seen before (Fig. 3C) (Dhingra *et al.*, 2021).

Compared with *rfa1-zm2* cells, *srs2-ΔPIM rfa1-zm2* and *srs2-3KR rfa1-zm2* cells showed increased percentages of cells transitioning into the G1 phase (Fig. 3C). The suppressive effects seen in both assays were stronger for *srs2-ΔPIM* than *srs2-3KR* as seen in genotoxicity assays (Fig. S1B; 3B, 3C). When assaying for chromatin RPA levels, we found that while *srs2-Δpim* showed an increase compared with the wild-type control, *rfa1-zm2* reversed this effect (Fig. S2). This data supports the Srs2 and RPA antagonism. Collectively, results from the above assays are consistent with each other and suggest that Srs2 binding to PCNA and its sumoylation contribute to RPA antagonism during DDC regulation.

srs2-ΔPIM is additive with a *slx4* mutant defective in DDC recovery

We found that *srs2-ΔPIM* and *srs2-3KR* mutants on their own behaved normally in the two DDC assays described above, which differs from *srs2Δ* cells that exhibit increased levels of Rad53 phosphorylation and reduced G1 entry (Fig. 3B, 3C) (Dhingra *et al.*, 2021). One plausible interpretation of this difference is that unlike *srs2Δ*, these partially defective *srs2* mutants only mildly impair Srs2-mediated RPA regulation during DDC downregulation, such that their defects can be compensated for by other DDC dampening systems. To test this idea, we examined the consequences of removing the Slx4-mediated anti-checkpoint function in *srs2-ΔPIM* cells. Slx4 is known to bind the scaffold protein Rtt107, and their complex can compete with the DDC protein Rad9 for binding to damaged chromatin, consequently disfavoring Rad9's role in promoting Rad53 phosphorylation (Ohouo *et al.*, 2010, Ohouo *et al.*, 2013). Slx4 uses an Rtt107 interaction motif (RIM) to bind Rtt107 and a previously established RIM mutant, $slx4^{RIM}$ (T423A, T424A, and S567A), abolishes Rtt107 binding without affecting other Slx4 protein attributes (Wan *et al.*, 2019). $slx4^{RIM}$ was tagged with a TAP tag at its C-terminal end and examined together with a control wherein the wild-type Slx4 was tagged in the same manner. Compared with the control, $slx4^{RIM}$ exhibited mild sensitivity toward CPT (Fig. 4A). Significantly, when *srs2-ΔPIM* was combined with $slx4^{RIM}$, the double mutant exhibited stronger CPT sensitivity compared with corresponding single mutants (Fig. 4A).

We further examined DDC levels when cells were exposed to CPT using both Rad53 phosphorylation and ability to timely exit G2/M as readouts. Compared with *SLX4-TAP* cells, $slx4^{RIM}$*-TAP* cells exhibited a 2-fold increase in Rad53 phosphorylation levels, consistent with a role of Slx4 in downregulating DDC (Fig. 4B). In *SLX4-TAP* background, *srs2-ΔPIM* led to 2-fold increase in Rad53 phosphorylation level (Fig. 4B). As cells containing untagged Slx4 and *srs2-ΔPIM* did not show Rad53 phosphorylation changes (Fig. 3B), tagging Slx4 appeared to sensitize *srs2-ΔPIM.* Significantly, the *srs2-ΔPIM* $slx4^{RIM}$*-TAP* double mutant exhibited further increase in Rad53 phosphorylation than either *srs2-ΔPIM* or $slx4^{RIM}$*-TAP* single mutant (Fig. 4B). Congruous with this finding, the *srs2-ΔPIM* $slx4^{RIM}$*-TAP* double mutant also reduced the percentage of cells entering G_1 compared with their single mutants after 2-hour treatment with CPT (Fig. 4C). Together, these three lines of evidence support the notion that defects in the Srs2-mediated DDC downregulation can be compensated for by Slx4-mediated mechanisms.

Srs2 binding to PCNA facilitates Srs2 sumoylation

We next addressed whether the two Srs2 features involved in RPA antagonism are functionally related. To this end, we tested if Srs2 binding to PCNA affected Srs2 sumoylation in cells. We confirmed that endogenous sumoylation of Srs2 could be detected in cell extracts after enriching SUMOylated proteins using 8His-tagged SUMO (8His-Smt3) (Fig. 5A). Briefly, proteins were extracted from cells under denaturing conditions to disrupt protein-protein

302 association and prevent desumoylation, and sumoylated proteins were enriched on Ni-NTA
303 (nickel-nitrilotriacetic acid) resin (Ulrich and Davies, 2009). Consistent with previous findings,
304 sumoylated forms of Srs2 in the Ni-NTA eluate were detected on immunoblots using an anti-
305 Srs2 antibody only when cells contained 8His-Smt3, where unmodified Srs2 was seen in the
306 presence or absence of 8His-Smt3 due to nonspecific binding to the resin (Fig. S3A) (Saponaro
307 *et al.*, 2010). These bands were only seen in wild-type cells but not *srs2*Δ cells (Fig. S3A). We
308 found that Srs2 sumoylation level was reduced in *srs2-3KR* strains in CPT conditions, as
309 expected from mutating the three major sumoylation sites (Fig. 5A) (Saponaro *et al.*, 2010).
310 Interestingly, *srs2-ΔPIM* cells exhibited a similar reduction in Srs2 sumoylation as seen in *srs2-*
311 *3KR* cells (Fig. 5A). This result suggests that Srs2 sumoylation largely depends on Srs2 binding
312 to PCNA, supporting the notion that the two events occur sequentially.
313
314
315 **Srs2 sumoylation peaks after maximal Mec1 activation and depends on Mec1**
316
317 While RPA can engage with ssDNA generated in different processes, such as transcription,
318 DNA repair, and DNA replication, only a subset of ssDNA regions is adjacent to 3'-junctions
319 loaded with PCNA. This is because PCNA loading requires an ssDNA and dsDNA junction site
320 with a 3' DNA end (Moldovan *et al.*, 2007). We thus reasoned that Srs2 binding to PCNA may
321 prevent Srs2 from removing RPA bound to ssDNA that is not flanked by PCNA, such as within
322 R-loop regions and negatively supercoiling DNA regions, both of which are generated
323 abundantly in CPT conditions due to topological stress (Pommier *et al.*, 2022). This could
324 provide a means for spatial control of Srs2's anti-RPA role. We explored whether this role could
325 also be regulated temporally. As the genetic data described above suggest that Srs2
326 sumoylation acts downstream of Srs2 binding to PCNA in antagonizing RPA, we examined the
327 timing of Srs2 sumoylation after CPT treatment.
328
329 We released G1 synchronized cells into media containing CPT and examined Srs2
330 sumoylation at several time points (Fig. 5B). A similar experimental scheme was used to
331 monitor the level of Mec1 activation using Rad9 phosphorylation as a readout (Fig. 5C).
332 Quantification of Srs2 sumoylated forms relative to its unmodified forms showed that its
333 sumoylation level peaked between 1.5 and 2 h after cells were released into CPT (Fig. 5D).
334 Quantification of phosphorylated forms of Rad9 relative to its unmodified form showed that
335 checkpoint activation peaked 1 hour after cell release (Fig. 5D). That checkpoint level peaked
336 before Srs2 sumoylation level peaked suggests a possible dependence of the latter on the
337 checkpoint. In testing this idea, we found that *mec1*Δ cells, which contain *sml1*Δ to support
338 viability (Zhao *et al.*, 1998), abolished Srs2 sumoylation (Fig. 5E). Neither *sml1*Δ alone nor
339 removal of Rad53 affected Srs2 sumoylation (Fig. 5E), suggesting that Mec1's effect on this
340 modification does not require the downstream Rad53 effector kinase. As Mec1 is not generally
341 required for protein sumoylation during the DNA damage response (Cremona *et al.*, 2012), its
342 involvement in Srs2 sumoylation presents a rather unique effect.
343
344
345 **Examination of Mec1-S1964 phosphorylation in Srs2-mediated DDC regulation**
346
347 The combined results that Srs2 sumoylation levels peak after Rad9 phosphorylation reaches
348 maximal level and that Srs2 sumoylation depends on Mec1 raised the possibility that Mec1
349 hyper-activation during the late part of the DNA damage response may favor Srs2's role in DDC
350 dampening. Recently, Mec1 protein bound to Ddc2 was shown to be auto-phosphorylated at
351 Ser1964 in a late part of the DNA damage response after a single DNA break is induced by the
352 HO endonuclease (Memisoglu *et al.*, 2019). Further, the phosphorylation-defective mutant

353 *mec1-S1964A* impaired checkpoint downregulation in this condition, leading to the model that
354 Mec1-S1964 phosphorylation contributes to DDC dampening at least after HO-induced break
355 (Memisoglu *et al.*, 2019). We thus tested whether Mec1-S1964 phosphorylation is also involved
356 in Srs2-mediated DDC regulation under CPT conditions.
357
358 First, we asked whether Mec1-S1964 phosphorylation occurs under CPT conditions
359 using a time course scheme similar to the one used in testing Srs2 sumoylation as described
360 above. Ddc2-bound Mec1 was recovered after immunoprecipitating Ddc2 at each timepoint and
361 the proteins were examined by immunoblotting. To detect Mec1-S1964 phosphorylation, we
362 used an antibody raised against the peptide containing this modification provided kindly by the
363 Haber lab (Memisoglu *et al.*, 2019). The antibody detected the Mec1 S1964 phosphorylation
364 band in immunoprecipitated fractions only when Ddc2 was Myc tagged but not when Ddc2 was
365 untagged (Fig. S3B). Further, the Mec1 S1964 phosphorylation band was largely abolished in
366 the *mec1-S1964A* cells (Fig. S3B; 6A). Given that the antibody also detects a closely spaced
367 background band (Fig. S3B; 6A), we calculated the relative level of Mec1 S1964
368 phosphorylation in each sample by normalizing to this band. Quantification results showed that
369 Mec1 S1964 phosphorylation level peaked around the same time as seen for Rad9
370 phosphorylation, which was 1 hour after CPT treatment (Fig. 6A).
371
372 After confirming that Mec1 S1964 phosphorylation also took place under CPT
373 conditions, we tested whether *mec1-S1964A* or the phosphorylation-mimetic mutant, *mec1-*
374 *S1964E*, influenced *rfa1-zm2* or *srs2* growth on media containing CPT. If Mec1 S1964
375 phosphorylation aids Srs2-mediated RPA antagonism in CPT, we would expect *mec1-S1964A*
376 to behave similarly to *srs2* mutants in rescuing *rfa1-zm2* CPT sensitivity, while *mec1-S1964E*
377 should have the opposite effects. We found that *mec1-S1964A,* which showed normal CPT
378 resistance on its own, did not affect the growth of *rfa1-zm2* cells on CPT-containing media (Fig.
379 6B). *mec1-S1964A* also did not influence the growth of *srs2-ΔPIM* and *srs2-3KR* cells
380 regardless of *rfa1-zm2* (Fig. 6B; S4A).
381
382 Though *mec1-S1964E* on its own did not cause CPT sensitivity, it led to slight but
383 reproducible slow growth in cells containing *srs2-3KR* and *srs2-ΔPIM* with or without *rfa1-zm2*
384 (Fig. S4B). We found that neither *mec1-S1964A* nor *mec1-S1964E* affected Srs2 sumoylation
385 levels (Fig. S4C). Thus, Mec1, but not its S1964 phosphorylation, is required for Srs2
386 sumoylation. These data provide evidence that even though an HO-induced DNA break and
387 CPT treatment both induce Mec1 S1964 phosphorylation, this modification appears to not affect
388 Srs2-mediated DDC dampening in the latter situation.
389
390
391 **Genetic data suggest that known RPA phosphorylation sites do not affect DDC recovery**
392
393 While we mainly focused on the identification of Srs2 features that contribute to RPA
394 antagonism during DDC regulation, we also considered the possibility that certain regulatory
395 RPA features may contribute to this control as well. RPA is known to be phosphorylated by
396 Mec1 (Chen *et al.*, 2010, Faca *et al.*, 2020, Lanz *et al.*, 2021). We thus tested whether Mec1-
397 mediated phosphorylation may render RPA more susceptible to be removed from ssDNA by
398 Srs2. To this end, we mutated previously identified Mec1 phosphorylation sites on the Rfa1 and
399 Rfa2 subunits. These include Rfa1 Ser178 and three sites on Rfa2 (S122, S187, S189)
400 (Albuquerque *et al.*, 2015, Chen *et al.*, 2010). We generated corresponding non-
401 phosphorylatable mutants, *rfa1-S178A* and *rfa2-3SA (*S122A, S187A, and S189A), and
402 phosphomimetic mutants, *rfa1-S178D* and *rfa2-3SD*.
403

404 Using genetic suppression as a readout for possible involvement of RPA mutants in
405 Srs2-based DDC regulation, we examined the interactions between the mutants affecting RPA
406 phosphorylation sites as described above and *srs2*Δ. If RPA phosphorylation promote its
407 removal by Srs2, the *SD* mutants may show suppressive interactions with *srs2*Δ, while *SA*
408 mutants would behave like *srs2* mutants. We found that neither *rfa1-S178D* nor *S178A*, both of
409 which showed normal CPT resistance on their own, affected *srs2*Δ cell growth on CPT-
410 containing media (Fig. 6C). In contrast, *rfa2-3SD* or *rfa2-3SA,* which also behaved like wild-type
411 regarding CPT sensitivity, sensitized *srs2*Δ growth on CPT-containing media (Fig. 6D). This
412 negative genetic interaction contrasts with the positive interaction seen between *srs2*Δ and *rfa1-*
413 *zm2* or *rfa1-t33* (Fig. S1A) (Dhingra *et al.*, 2021). The differential Srs2 genetic interactions
414 among distinct RPA alleles likely reflect the multifunctional natures of Srs2 and RPA.
415 Collectively, these analyses suggest that the known phosphorylation sites on RPA are unlikely
416 to be involved in Srs2-based DDC regulation.
417
418
419 **Discussion**
420
421 Timely termination of DDC is crucial for cell survival, yet the underlying mechanisms are not well
422 understood. Here we address this question in the context of Srs2-mediated DDC dampening in
423 budding yeast. Our previous work reports a requirement of Srs2's ATPase activity in this role;
424 here we examined additional Srs2 features involved in either binding to other proteins or post-
425 translational modifications. Our results suggest that among the examined features, Srs2 binding
426 to PCNA and its sumoylation are involved in RPA antagonism during DDC downregulation. We
427 showed that mutants impairing these features, namely *srs2*Δ*-PIM* and *srs2-3KR*, suppressed
428 both DDC abnormalities and CPT sensitivity of *rfa1-zm2* cells. Interestingly, these features are
429 functionally linked, since optimal Srs2 sumoylation requires its binding to PCNA. Further, the
430 Srs2 sumoylation level peaks after Mec1 activity reaches its maximum and that Mec1 is
431 required for this modification. We posit a model that can interpret previous and current data. In
432 this model, Srs2 removal of RPA is favored at a subset of ssDNA-containing regions that have
433 proximal PCNA (Fig. 7, top). PCNA recruits Srs2 toward the adjacent RPA-ssDNA filament, and
434 promotes Srs2 sumoylation together with hyperactive Mec1 to foster downregulation of the
435 Mec1 checkpoint (Fig. 7, bottom).
436
437 RPA-ssDNA filaments can be separated into two groups from the perspective of PCNA
438 loading status. The first group contains 3' DNA end at the ss-dsDNA junction that permit PCNA
439 loading (Fig. 7, top, green). These regions can include ssDNA gaps produced from perturbed
440 replication (Sogo *et al.*, 2002) or from excision and repair of trapped Top1 (Sun *et al.*, 2020).
441 Due to PCNA proximity, this group of ssDNA regions can favor Srs2 recruitment and RPA
442 removal. Since they often also contain 5' DNA ends required for loading the 9-1-1 complex
443 (Majka *et al.*, 2006), these sites can be ideal for Srs2's action in checkpoint dampening.
444 Biochemical data suggested that PCNA is loaded exclusively at the 3' DNA ends at ssDNA-
445 dsDNA junctions by the RFC complex in the presence of RPA, though PCNA loading could
446 occur at 5' DNA ends in the absence of RPA (Ellison and Stillman, 2003, Majka *et al.*, 2006).
447 We thus do not exclude the possibility that ssDNA-dsDNA junctions containing 5' DNA ends,
448 such as those formed at resected DNA breaks, may also allow Srs2-based RPA regulation. The
449 second group of ssDNA regions are devoid of DNA ends thus PCNA loading (Fig. 7, top, white).
450 These regions can be within R-loops or negatively supercoiled regions, which are induced by
451 CPT treatment due to increased topological stress associated with the depletion of the
452 functional pool of Top1 (Pommier *et al.*, 2022). These regions are unlikely to contain DNA ends
453 at ss-dsDNA junctions; thus, RPA there mainly supports DNA protection and repair and not
454 DDC. We reason that these ssDNA sites can be shielded from Srs2 removal of RPA to allow

455 better repair and protection. The notion that ssDNA regions close to PCNA are preferred for
456 Srs2 anti-checkpoint action provides a rationale for how Srs2 could remove RPA at some sites
457 while minimizing unnecessary RPA loss from other sites. Quantitative assessment of RPA
458 residence on DNA and genome-wide mapping of Srs2 action sites in the future can further test
459 the proposed models and provide more clarity. Regardless, results presented in this work
460 provide evidence for the model that Srs2 can distinguish between two types of ssDNA regions
461 using PCNA proximity as a guide for RPA removal.
462
463 Genetic analysis showed that *srs2Δ-PIM* also suppressed *rfa1-zm2* sensitivity toward
464 MMS, though to a less degree as seen in CPT conditions. While more than one factor could
465 contribute to this difference, we note that CPT only activates the DNA damage checkpoint, while
466 MMS additionally induces the DNA replication checkpoint (Menin *et al.*, 2018, Redon *et al.*,
467 2003, Tercero *et al.*, 2003). It is thus possible that the Srs2-RPA antagonism is more important
468 for the DNA damage checkpoint compared with the DNA replication checkpoint. With this said,
469 we do not exclude the possibility that the Srs2-RPA antagonism may also be relevant to specific
470 forms of DNA repair. Further investigation of this possibility among others will shed light on
471 differential suppressive effects seen here.
472
473 An involvement of Srs2-PCNA binding in Srs2-based RPA regulation could compensate
474 for a lack of interaction between Srs2 and RPA. This scenario differs from Srs2-based Rad51
475 stripping that requires Srs2 interacts with Rad51 (Antony *et al.*, 2009, Colavito *et al.*, 2009,
476 Krejci *et al.*, 2003). It is thus likely that though both the anti-recombinase and anti-checkpoint
477 roles of Srs2 benefit from selectivity of protein to be stripped from DNA, they are achieved via
478 different means. Our previous work has provided several lines of evidence to support that
479 Rad51 removal by Srs2 can be functionally separable from the Srs2-RPA antagonism (Dhingra
480 *et al.*, 2021). Consistent with this conclusion, deleting the Rad51 binding domain in Srs2 had no
481 effect on *rfa1-zm2* phenotype in CPT (Fig. 2D). This contrasts with mutating the PCNA binding
482 and the sumoylation sites of Srs2, which suppressed *rfa1-zm2* defects (Fig. 2C). This data
483 provides additional evidence that Srs2 regulation of Rad51 is separable from the Srs2-RPA
484 antagonism at genetic level. For this reason, the Srs2-based Rad51 function was not further
485 examined in this study. However, future studies to address how Srs2 regulates RPA and Rad51
486 in different manners and whether there is a crosstalk between them in specific contexts will help
487 to generate a more comprehensive understanding of both roles of Srs2.
488
489 Previous studies have suggested that both PIM and SIM aid Srs2 recruitment to
490 sumoylated form of PCNA (Papouli *et al.*, 2005, Pfander *et al.*, 2005). Our data reveal that at
491 least in CPT conditions, Srs2-PIM, but not Srs2-SIM, is involved in RPA regulation. This
492 observation is congruent with phenotypic differences between Srs2's PIM and SIM seen in other
493 studies and here, such as a much stronger genotoxic sensitivity of the latter (Fig. S1A) (Fan *et*
494 *al.*, 2023, Kolesar *et al.*, 2016, Kolesar *et al.*, 2012). Considering that only a small percentage of
495 PCNA is sumoylated and mainly during S phase (Papouli *et al.*, 2005, Pfander *et al.*, 2005), it is
496 probably advantageous for Srs2 not being restricted to sumoylated PCNA in order to achieve
497 efficiency in RPA regulation.
498
499 How could Srs2 binding to PCNA helps Srs2 sumoylation? While a full answer awaits
500 future studies, we speculate that this interaction may render Srs2 more permissive for
501 sumoylation and/or position Srs2 in proximity with its sumoylation E3 ligase Siz2 that binds RPA
502 (Chung and Zhao, 2015, Kolesar *et al.*, 2012). Considering that Mec1, Ddc2, and RPA contain
503 SUMO interaction motifs (SIMs) (Psakhye and Jentsch, 2012), it is possible that sumoylation
504 could help enrich Srs2 at ssDNA-RPA sites via SIM interactions, though other effects are
505 possible. Compared with *srs2-3KR*, *srs2-ΔPIM* showed better suppression of *rfa1-zm2* defects.

506 This indicates that during RPA regulation, PCNA plays additional roles besides promoting Srs2
507 sumoylation.
508
509 We found that Srs2 sumoylation in cells also requires Mec1, which does not promote
510 sumoylation in general (Cremona *et al.*, 2012). On the contrary, Mec1 loss causes increased
511 sumoylation levels of multiple proteins (Cremona *et al.*, 2012). It is currently unclear how Mec1
512 can specifically promote Srs2 sumoylation, but this may involve Mec1-mediated phosphorylation
513 of SUMO substrates and/or enzymes. A requirement of Mec1 for Srs2 sumoylation and the
514 dynamic nature of sumoylation suggest that Srs2 sumoylation may be a potential timing
515 regulator. It is possible that hyperactivation of Mec1 favors Srs2 sumoylation that may aid its
516 own downregulation. While fully testing this idea requires time-course phosphor-proteomic
517 studies under genotoxin treatment, we examined a Mec1 auto-phosphorylation site implicated in
518 its downregulation after induction of a single DNA break (Memisoglu *et al.*, 2019). We did not
519 find evidence that it is involved in Mec1 dampening in CPT condition, raising the possibility that
520 distinct mechanisms may be used in different genomic stress conditions. We also found that two
521 phosphorylation sites on Srs2 that showed Mec1 dependency in proteomic studies had no effect
522 in the CPT situation (Albuquerque *et al.*, 2015, Faca *et al.*, 2020); however we note that these
523 sites do not fit with the typical S/TQ Mec1 consensus sites, thus may not be the bona fide Mec1
524 sites. Other phosphorylation sites examined here include five Mec1 sites on Rfa1 and Rfa2
525 (Albuquerque *et al.*, 2015, Chen *et al.*, 2010). Genetic analyses did not support their roles in the
526 Srs2 and RPA antagonism. Thus, comprehensively map DDC kinase phosphorylation sites on
527 Srs2, RPA, and possibly their regulators, such as the RPA chaperone Rtt105 (Li *et al.*, 2018),
528 will be needed to identify targets of the kinases that can facilitate Srs2-based RPA regulation.
529
530 While we provide multiple lines of evidence in support of the involvement of Srs2 binding
531 to PCNA and its sumoylation in RPA regulation during DDC downregulation, *srs2-ΔPIM* or *-3KR*
532 alone behaved normally in checkpoint assays. A lack of defect here can be due to buffering
533 effects, both from not-yet characterized Srs2 features and from other checkpoint dampening
534 pathways. In addressing the former possibility, we tested the separation pin of Srs2 (Y775).
535 This residue was shown to be key for the Srs2's helicase activity *in vitro* in a report that was
536 published during the revision of our work (Meir *et al.*, 2023). We found that *srs2-Y775A* that
537 severely compromised the Srs2 helicase activity rescued *rfa2-zm2* sensitivity to CPT (Fig. S5).
538 This result suggests that Y775 could contribute to *in vivo* RPA removal; future examination of
539 this feature in conjunction with PCNA binding and sumoylation, can extend our understanding of
540 Srs2-mediated DDC regulation. We also provided evidence for the latter possibility, since *srs2-*
541 *ΔPIM* or *-3KR* showed additive phenotype when combined with a *slx4* mutant defective in DDC
542 dampening function. The presence of multiple checkpoint-dampening factors that target different
543 checkpoint modules highlights the importance of the process. Recent demonstration of other
544 DNA helicases, such as the human HELB, HELQ, and BLM proteins, in stripping of RPA from
545 ssDNA *in vitro* suggests that Srs2-like checkpoint downregulation may present in human cells
546 as well (Hormeno *et al.*, 2022, Jenkins *et al.*, 2021, Shorrocks *et al.*, 2021). Since RPA-ssDNA
547 binding not only plays a key role in checkpoint, but also in many other processes, the Srs2
548 features uncovered here may help to better understand how RPA dynamics is controlled by
549 helicases and other factors during additional processes beyond DDC.
550
551
552 **Methods**
553
554 **Yeast strains and genetic techniques.** Standard procedures were used for cell growth and
555 media preparation. The strains used in this work are listed in Table S1 and are isogenic to
556 W1588-4C, a *RAD5* derivative of W303 (Zhao and Blobel, 2005). Mutant alleles of *srs2*, *rfa1*,

557 *rfa2* and *mec1* used in this work were generated by CRISPR-Cas9-based gene replacement,
558 except for *srs2-3KR* that was introduced using a PCR-based method (DiCarlo *et al.*, 2013). All
559 mutations were verified by sequencing. Standard procedures were used for tetrad analyses and
560 genotoxin testing. For each assay, at least two biological duplicates were used per each
561 genotype. Cells were grown at 30 ºC unless otherwise stated.
562
563 **Cell synchronization and cell cycle analyses.** Cells from log-phase cultures were treated with
564 5 µg/mL α factor (GenScript RP01002) for 1 h, followed by an additional 2.5 µg/mL α factor for
565 30 min. When at least 95% cells were arrested in G1 phase based on the percentage of
566 unbudded cells, they were released into yeast extract–peptone–dextrose (YPD) media
567 containing 100 µg/mL Protease (Millipore 53702) and 16 µg/mL CPT (Sigma C9911) for 2 h.
568 Cell cycle progression was monitored by standard flow cytometry analyses as described
569 previously (Zhao and Rothstein, 2002). To derive percentage of G1 cells in Figure 3B, the G1
570 region of the "G1 sample" was used to demarcate the G1 region of the "CPT 2h" sample of the
571 same strain in the same experiment.
572
573 **Protein extraction using trichloroacetic acid (TCA).** To examine the protein levels of Srs2,
574 the phosphorylation form of Rad53, and Rad9, cell extracts were prepared as reported (Regan-
575 Mochrie *et al.*, 2022) . Briefly, 2×10^8 cells were collected at indicated time points. Cell pellets
576 were resuspended in 20% TCA and lysed by glass bead beating. The lysate was then
577 centrifuged to remove supernatant. Precipitated proteins were suspended in Laemmli buffer (65
578 mM Tris-HCl at pH 6.8, 2% SDS, 5% 2-mercaptoethanol, 10% glycerol, 0.025% bromophenol
579 blue) with 2 M Tris added to neutralize the solution. Prior to loading, samples were boiled for 5
580 min and spun down at 14,000 rpm for 10 min to remove insoluble materials. Samples were
581 separated on 4-20% Tris-glycine gels (Bio-Rad 456-1096) to examine Srs2 level and
582 phosphorated Rad53 form or 7% Tris-acetate gels (Thermo Fisher EA03555) to detect Rad9
583 phosphorylation.
584
585 **Detection of Srs2 sumoylation.** Sumoylated proteins were pulled down from cells containing
586 8His-tagged SUMO expressed from its endogenous locus using the standard Ni-NTA pull-down
587 method as previously described (Ulrich and Davies, 2009). Briefly, protein extracts prepared in
588 55% TCA were incubated in buffer A (6 M guanidine HCl, 100 mM sodium phosphate at pH 8.0,
589 10 mM Tris-HCl at pH 8.0) with rotation for 1 h at room temperature. The cleared supernatant
590 was obtained after centrifuging for 20 min and was then incubated overnight at room
591 temperature with Ni-NTA resin (Qiagen 30210) in the presence of 0.05% Tween-20 and 4.4 mM
592 imidazole with rotation. Beads were washed twice with buffer A supplemented with 0.05%
593 Tween 20 and then four times with buffer C (8 M urea, 100 nM sodium phosphate at pH 6.3, 10
594 mM Tris-HCl at pH 6.3) supplemented with 0.05% Tween 20. Proteins were eluted from the
595 beads using HU buffer (8 M urea, 200 mM Tris-HCl at pH 6.8, 1 mM EDTA, 5% SDS, 0.1%
596 bromophenol blue, 1.5% DTT, 200 mM imidazole). Samples were loaded onto NuPAGE™ 3–
597 8% Tris-acetate gels (Thermo Fisher EA03752) for immunoblotting to detect both sumoylated
598 and unmodified Srs2. Equal loading was verified using Ponceau S staining.
599
600 **Detection of Mec1 S1964 phosphorylation during CPT treatment.** G1-arrested cells were
601 filtered and resuspended in prewarmed YPD media containing 16 µg/mL CPT to allow entry into
602 S phase. Samples were collected at indicated time points. Cells were disrupted by glass bead
603 beating in lysis buffer, followed by centrifugation at 20,000 g for 15 min to obtain whole-cell
604 extract. The lysis buffer consisted of 25 mM K-HEPES (pH 7.6), 100 mM NaCl, 100 mM K-
605 glutamate, 5 mM $Mg(OAc)_2$, 0.02% NP40, and 0.5% Triton X-100 supplemented by protease
606 inhibitor cocktail (Sigma P8215) and Complete Ultra EDTA-free protease inhibitor (Roche
607 11836145001). The activated form of Mec1 was enriched by immunoprecipitating myc-tagged

608 Ddc2 using Protein A beads and an anti-Myc antibody (Thermo Fisher 9E10) for 2–4 h at 4°C.
609 Beads were washed five to six times with lysis buffer, and proteins were eluted using Laemmli
610 buffer (65 mM Tris-HCl at pH 6.8, 2% SDS, 5% 2-mercaptoethanol, 10% glycerol, 0.025%
611 bromophenol blue). After boiling for 5 min, eluted proteins were loaded onto NuPAGE™ 3–8%
612 Tris-acetate gels for SDS-PAGE and subsequent immunoblotting analyses.
613
614 **Immunoblotting analysis and antibodies.** After SDS-PAGE, proteins were transferred to a
615 0.2-µm nitrocellulose membrane (GE, #G5678144) for immunoblotting. Pgk1 was used as a
616 loading control. Antibodies used were anti-myc (Thermo, Fisher 9E10). anti-Srs2 (Santa Cruz,
617 yC-18), anti-Pgk1 (Invitrogen, 22C5D8), F9 (a kind gift from Marco Foiani and Daniele Piccini,
618 The FIRC Institute of Molecular Oncology, Milan, Italy) (Pellicioli *et al.*, 2001), anti-Rad9 (a kind
619 gift from John Petrini, MSKCC, NY, USA) (Usui *et al.*, 2009), anti-Mec1-S1964-p (a kind gift
620 from James E. Haber, Brandeis University, MA, USA) (Memisoglu *et al.*, 2019). Validation of
621 antibodies is provided either by the manufacturers or in the cited references. Membranes were
622 scanned with a Fujifilm LAS-3000 luminescent image analyzer, which has a linear dynamic
623 range of 10^4. The signal intensities of non-saturated bands were measured using ImageJ
624 software. For graphs, mean and SD are depicted.
625
626 **Statistical analyses.** Pairwise comparison was conducted, and statistical differences were
627 determined using two-sided Student's t-test as indicted in the graphs and figure legends.
628
629 **Acknowledgments.** We thank Drs. James Haber, Marco Foiani, Daniele Piccini, John Petrini
630 for sharing antibodies, and Tzippora Chwat-Edelstein for critical reading of the manuscript. X.Z.
631 is supported by National Institute of General Medical Sciences (NIGMS) grants R35GM145260.
632
633 **Author contributions**: All authors were involved in research design and data analyses, J. F., N.
634 D., T. Y., and V. Y. performed research. J. F. and X.Z. wrote the paper with all authors' input.
635
636 **Competing interest statement**: The authors declare no competing interests.
637
638 **Figure Legends.**
639
640 **Figure 1. Regulatory features of Srs2 and corresponding mutants.**
641 (A) Schematic of Srs2 protein domains, regulatory features, and mutations affecting each of its
642 features. Cdk1 phosphorylation sites depicted here include T604, S698, S879, S893, S938,
643 S950, and S965 (Chiolo *et al.*, 2005). Potential Mec1 phosphorylation sites include S890
644 and S933 (Albuquerque *et al.*, 2015, Faca *et al.*, 2020). Sumoylation sites mapped
645 previously include K1081, K1089, and K1142 (Saponaro *et al.*, 2010). Protein-interaction
646 domains or motifs include the Rad51 binding domain (BD), PCNA Interaction Motif (PIM),
647 and SUMO Interaction Motif (SIM) (Colavito *et al.*, 2009, Kolesar *et al.*, 2016, Kolesar *et al.*,
648 2012). The residues for these domains are indicated. Mutant alleles disabling each of these
649 features are included in the parentheses.
650 **(B)** Mutations affecting Srs2 features do not affect Srs2 protein level. Protein extracts were
651 prepared from asynchronous cells. Srs2 was examined using anti-Srs2 antibody by
652 immunoblotting. Srs2 levels in each mutant were first normalized to the Pgk1 loading control
653 and then to those in wild-type cells. Mean of two biological isolates per genotype is graphed
654 with error bars representing standard deviation (SD). No statistical differences were seen
655 when compared the Srs2 protein level between the wild-type (WT) control and each of the
656 indicated mutants based on student t-test.
657
658

659 **Figure 2. Srs2 PCNA binding and sumoylation are involved in suppressing *rfa1* mutants**
660 (A) Schematic to show that Srs2's roles in checkpoint dampening (anti-checkpoint for simplicity)
661 and DNA repair, both of which contribute to genotoxin resistance.
662 (B) Schematic to highlight the mutual suppressive relationship between *srs2*Δ and *rfa1* mutants
663 and the underlying effects on the RPA-ssDNA levels in cells.
664 (C) *srs2-ΔPIM* or *-3KR* suppresses *rfa1-zm2* sensitivity to CPT. A 10-fold serial dilution of cells
665 of the indicated genotypes were spotted and growth was assessed after incubation at 30°C
666 for 40 hours unless otherwise noted.
667 (D) Several *srs2* mutants did not suppress *rfa1-zm2* sensitivity to CPT. Experiments were
668 performed as in panel C.
669 (E) *srs2-ΔPIM* or *-3KR* suppresses *rfa1-t33* sensitivity to CPT. Top: schematic of the Rfa1
670 protein domains and *rfa1* mutant alleles. Bottom: *srs2-ΔPIM* or *-3KR* improved *CPT*
671 sensitivity of *rfa1-t33* cells. Experiments were performed as in panel C.
672
673
674 **Figure 3. *srs2-ΔPIM* and *-3KR* correct checkpoint abnormalities in *rfa1-zm2* cells.**
675 (A) A table summarizing DDC levels observed in *rfa1-zm2*, *srs2* null or partially defective
676 mutants, and their combined mutants in this work and in a previous study (Dhingra *et al.*,
677 2021) and interpretations.
678 (B) *srs2-ΔPIM* or *-3KR* reduces the levels of phosphorylated Rad53 in *rfa1-zm2* cells. Protein
679 extracts were examined after G1 cells were released into cycling in the presence of 16 ug/ml
680 CPT for 2 hours. Phosphorylated Rad53 (active form) was detected by the F9 antibody by
681 immunoblotting. Phosphorylated Rad53 signals in each indicated strain were compared to
682 the Pgk1 loading control and normalized to those of *rfa1-zm2*. Two biological isolates per
683 genotype were examined in two technical repeats and results are graphed with error bars
684 representing SD. Statistical analysis was performed using pairwise Student's t-test (*, p
685 <0.05; ***, p <0.001; ****, p <0.0001, and non-statistical significance is not marked)
686 (C) *srs2-ΔPIM* and *-3KR* allow better G1 entry of *rfa1-zm2* cells. Experiments were performed
687 as in panel A and samples were collected at indicated time points. FACS profiles of the
688 samples are shown at the top and percentages of G1 cells after 2 hours of CPT treatment
689 (CPT 2 h) are plotted at the bottom. Two biological isolates per genotype were examined in
690 two technique repeats and results are graphed with error bars representing SD. Statistical
691 analysis was performed and results are depicted as in panel B.
692
693 **Figure 4. *srs2-ΔPIM* and *slx4^{RIM}* are additively defective in DDC down-regulation.**
694 (A) The *srs2-ΔPIM*Δ *slx4^{RIM}* double mutant shows stronger CPT sensitivity than either single
695 mutant. Experiments are performed as in Figure 2C.
696 (B) *srs2-ΔPIM* and *slx4^{RIM}* are additive for increasing the level of phosphorylated Rad53 when
697 cells are treated with CPT. Experiments were conducted, and data are quantified as those
698 described in Figure 3B. Results from three biological isolates per genotype are graphed with
699 error bars representing SD. Statistical analysis was performed using pairwise Student's t-
700 test. *, p <0.05; **, p <0.01.
701 (C) *srs2-ΔPIM* and *slx4^{RIM}* are additive for reducing cells exiting from G2/M phase at 2 hours
702 post CPT treatment. Experiments were conducted and data are quantified as those
703 described in Figure 3C. Results from three biological isolates per genotype are graphed with
704 error bars representing SD. Statistical analysis was performed using pairwise Student's t-
705 test. *, p <0.05; **, p <0.01.
706
707 **Figure 5. Srs2 sumoylation depends on Srs2 PIM motif and the Mec1 kinase**
708 (A) Srs2 sumoylation level is reduced in *srs2-ΔPIM* cells. Samples were collected after CPT
709 treatment as in Figure 3A and sumoylated proteins were enriched as described in the text

710 and Methods. Sumoylated form of Srs2 (Srs2-Su) migrated slower than unmodified Srs2 on
711 gel and both were detected using anti-Srs2 antibody in immunoblotting. Equal loading is
712 indicated by Ponceau-S stain (Stain). The levels of sumoylated Srs2 relative to those of
713 unmodified Srs2 were normalized to wild-type cells and plotted. Two biological isolates per
714 genotype were examined in two technique repeats and results are graphed with error bars
715 representing SD. Statistical analysis was performed using pairwise Student's t-test. *, p
716 <0.05.
717 (B) Srs2 sumoylation level during CPT treatment. Samples were collected as described in
718 Figure 3B. Experiments were conducted, and immunoblotting data is presented as those in
719 panel A. Time 0 samples are G1 cells before CPT treatment. FACS analysis at
720 corresponding time points are included below the plot.
721 (C) Rad9 phosphorylation level during CPT treatment. Samples used in panel B were examined
722 for Rad9 phosphorylation using an anti-Rad9 antibody. Unmodified and phosphorylated
723 (Rad9-p) Rad9 forms are indicated. FACS analysis at corresponding time points are
724 indicated below blots.
725 (D) Quantification of Srs2 sumoylation and Rad9 phosphorylation level changes during CPT
726 treatment. Srs2 sumoylation signals were normalized based on unmodified form. Values at
727 each timepoint were relative to that of G1 sample (Time 0) before CPT treatment, and fold
728 changes were indicated on left y-axis. Rad9 signals were normalized to non-modified form
729 and percentage of phosphorylated form were indicated on right y-axis. Results from three
730 biological isolates per genotype are graphed.
731 (E) Mec1 is required for Srs2 sumoylation. Experiments were performed and data are presented
732 as in panel A.
733
734
735 **Figure 6. Mec1 and RPA phosphorylation did not link to Srs2 anti-checkpoint function.**
736 (A) Mec1 autophosphorylation at S1964 during CPT treatment. Samples were collected as
737 described in Figure 3B. Ddc2-myc was immunoprecipitated and the associated Mec1 was
738 co-purified. The anti-Mec1-S1964-p antibody detected the phosphorylated form of Mec1 and
739 a non-specific band (*). Quantification below the blot was based on results from two
740 biological isolates.
741 (B) *mec1-S1964A* did not rescue *rfa1-zm2* sensitivity toward CPT. Experiments were performed
742 as in Figure 2C.
743 (C) Examination of the *rfa1-S178A* and *-S178D* mutants. Top: schematic of the Rfa1 protein
744 domains and position of Ser178. ssDNA binding domain (DBD) A-C are shown. Bottom,
745 *rfa1-S178A* and *-S178D* had no effect on *srs2*Δ's sensitivity to CPT. Experiments were
746 performed as in Figure 2C.
747 (D) Examination of the *rfa2-3SA* and *-3SD* mutants. Top, schematic of the Rfa2 protein domains
748 and position of Ser122, Ser187 and Ser189 mutated in *rfa2-3SA* and *-3SD*. ssDNA binding
749 domain (DBD)-D is indicated. Bottom, *rfa2-3SA* has no effect on *srs2*Δ's sensitivity toward
750 CPT while *rfa2-3SD* showed additive effect. Experiments were performed as in Figure 2C.
751
752
753 **Figure 7. A working model for the regulation of Srs2-mediated checkpoint dampening.**
754 RPA-coated ssDNA regions generated from multiple DNA metabolic processes include those
755 without proximal PCNA, such as ssDNA within R-loops and negatively supercoiled regions, and
756 those with proximal PCNA, such as ssDNA gaps associated with perturbed DNA replication or
757 repair. In latter situations, the resultant RPA-ssDNA can recruit the Mec1/Ddc2 kinase complex.
758 Mec1 is subsequently activated by other DDC proteins, such as the 9-1-1 complex that
759 demarcates the 5' end junctions adjacent to ssDNA regions (not drawn). After DDC is activated
760 for a prolonged period, Srs2 recruited to PCNA that demarcates the 3' end junction flanking the

761 ssDNA regions can be sumoylated. Srs2 sumoylation level increases as Mec1 activation
762 heightens and can result in more efficient RPA removal, leading to Mec1 downregulation.
763
764
765
766

767 **References:**

768 Albuquerque CP, Yeung E, Ma S, Fu T, Corbett KD and Zhou H (2015) A chemical and enzymatic
769 approach to study site-specific sumoylation *PLoS One* 10: e0143810

770 Antony E, Tomko EJ, Xiao Q, Krejci L, Lohman TM and Ellenberger T (2009) Srs2 disassembles Rad51
771 filaments by a protein-protein interaction triggering ATP turnover and dissociation of Rad51 from DNA *Mol*
772 *Cell* 35: 105-115

773 Armstrong AA, Mohideen F and Lima CD (2012) Recognition of SUMO-modified PCNA requires tandem
774 receptor motifs in Srs2 *Nature* 483: 59-63

775 Bronstein A, Bramson S, Shemesh K, Liefshitz B and Kupiec M (2018) Tight Regulation of Srs2 Helicase
776 Activity Is Crucial for Proper Functioning of DNA Repair Mechanisms *G3* 8: 1615-1626

777 Chen SH, Albuquerque CP, Liang J, Suhandynata RT and Zhou H (2010) A proteome-wide analysis of
778 kinase-substrate network in the DNA damage response *J Biol Chem* 285: 12803-12812

779 Chiolo I, Carotenuto W, Maffioletti G, Petrini JH, Foiani M and Liberi G (2005) Srs2 and Sgs1 DNA
780 helicases associate with Mre11 in different subcomplexes following checkpoint activation and CDK1-
781 mediated Srs2 phosphorylation *Mol Cell Biol* 25: 5738-5751

782 Chung I and Zhao X (2015) DNA break-induced sumoylation is enabled by collaboration between a
783 SUMO ligase and the ssDNA-binding complex RPA *Genes Dev* 29: 1593-1598

784 Colavito S, Macris-Kiss M, Seong C, Gleeson O, Greene EC, Klein HL, Krejci L and Sung P (2009)
785 Functional significance of the Rad51-Srs2 complex in Rad51 presynaptic filament disruption *Nucleic*
786 *Acids Res* 37: 6754-6764

787 Cremona CA, Sarangi P, Yang Y, Hang LE, Rahman S and Zhao X (2012) Extensive DNA damage-
788 induced sumoylation contributes to replication and repair and acts in addition to the Mec1 checkpoint *Mol*
789 *Cell* 45: 422-432

790 Deng SK, Gibb B, de Almeida MJ, Greene EC and Symington LS (2014) RPA antagonizes
791 microhomology-mediated repair of DNA double-strand breaks *Nat Struct Mol Biol* 21: 405-412

792 Dhingra N, Kuppa S, Wei L, Pokhrel N, Baburyan S, Meng X, Antony E and Zhao X (2021) The Srs2
793 helicase dampens DNA damage checkpoint by recycling RPA from chromatin *Proc Natl Acad Sci U S A*
794 118: e2020185118

795 DiCarlo JE, Norville JE, Mali P, Rios X, Aach J and Church GM (2013) Genome engineering in
796 Saccharomyces cerevisiae using CRISPR-Cas systems *Nucleic Acids Res* 41: 4336-4343

797 Elledge SJ (1996) Cell cycle checkpoints: preventing an identity crisis *Science* 274: 1664-1672

798 Ellison V and Stillman B (2003) Biochemical characterization of DNA damage checkpoint complexes:
799 clamp loader and clamp complexes with specificity for 5' recessed DNA *PLoS Biol* 1: E33

800 Enoch T, Carr AM and Nurse P (1992) Fission yeast genes involved in coupling mitosis to completion of
801 DNA replication *Genes Dev* 6: 2035-2046

802 Faca VM, Sanford EJ, Tieu J, Comstock W, Gupta S, Marshall S, Yu H and Smolka MB (2020)
803 Maximized quantitative phosphoproteomics allows high confidence dissection of the DNA damage
804 signaling network *Sci Rep* 10: 18056

805 Fan J and Pavletich NP (2012) Structure and conformational change of a Replication Protein A
806 heterotrimer bound to ssDNA *Genes Dev* 26: 2337-2347

807 Fan L, Zhang W, Rybchuk J, Luo Y and Xiao W (2023) Genetic dissection of budding yeast PCNA
808 mutations responsible for the regulated recruitment of Srs2 helicase *mBio* 14: e0031523

809 Fiorani S, Mimun G, Caleca L, Piccini D and Pellicioli A (2008) Characterization of the activation domain
810 of the Rad53 checkpoint kinase *Cell Cycle* 7: 493-499

811 Foiani M, Pellicioli A, Lopes M, Lucca C, Ferrari M, Liberi G, Muzi Falconi M and Plevani P (2000) DNA
812 damage checkpoints and DNA replication controls in Saccharomyces cerevisiae *Mutat Res* 451: 187-196

813 Harrison JC and Haber JE (2006) Surviving the breakup: the DNA damage checkpoint *Annu Rev Genet*
814 40: 209-235

815 Hartwell LH and Weinert TA (1989) Checkpoints: controls that ensure the order of cell cycle events
816 *Science* 246: 629-634

817 Hormeno S, Wilkinson OJ, Aicart-Ramos C, Kuppa S, Antony E, Dillingham MS and Moreno-Herrero F
818 (2022) Human HELB is a processive motor protein that catalyzes RPA clearance from single-stranded
819 DNA *Proc Natl Acad Sci U S A* 119: e2112376119

820 Jenkins T *et al* (2021) The HelQ human DNA repair helicase utilizes a PWI-like domain for DNA loading
821 through interaction with RPA, triggering DNA unwinding by the HelQ helicase core *NAR Cancer* 3:
822 zcaa043

823 Kolesar P, Altmannova V, Silva S, Lisby M and Krejci L (2016) Pro-recombination Role of Srs2 Protein
824 Requires SUMO (Small Ubiquitin-like Modifier) but Is Independent of PCNA (Proliferating Cell Nuclear
825 Antigen) Interaction *J Biol Chem* 291: 7594-7607

826 Kolesar P, Sarangi P, Altmannova V, Zhao X and Krejci L (2012) Dual roles of the SUMO-interacting motif
827 in the regulation of Srs2 sumoylation *Nucleic Acids Res* 40: 7831-7843

828 Krejci L, Van Komen S, Li Y, Villemain J, Reddy MS, Klein H, Ellenberger T and Sung P (2003) DNA
829 helicase Srs2 disrupts the Rad51 presynaptic filament *Nature* 423: 305-309

830 Lanz MC, Dibitetto D and Smolka MB (2019) DNA damage kinase signaling: checkpoint and repair at 30
831 years *EMBO J* 38: e101801

832 Lanz MC, Yugandhar K, Gupta S, Sanford EJ, Faca VM, Vega S, Joiner AMN, Fromme JC, Yu H and
833 Smolka MB (2021) In-depth and 3-dimensional exploration of the budding yeast phosphoproteome *EMBO*
834 *Rep* 22: e51121

835 Li S *et al* (2018) Rtt105 functions as a chaperone for Replication Protein A to preserve genome stability
836 *EMBO J* 37: e99154

837 Majka J, Binz SK, Wold MS and Burgers PM (2006) Replication protein A directs loading of the DNA
838 damage checkpoint clamp to 5'-DNA junctions *J Biol Chem* 281: 27855-27861

839 Marechal A and Zou L (2015) RPA-coated single-stranded DNA as a platform for post-translational
840 modifications in the DNA damage response *Cell Res* 25: 9-23

841 Meir A, Raina VB, Rivera CE, Marie L, Symington LS and Greene EC (2023) The separation pin
842 distinguishes the pro- and anti-recombinogenic functions of *Saccharomyces cerevisiae* Srs2 *Nat*
843 *Commun* 14: 8144

844 Memisoglu G, Lanz MC, Eapen VV, Jordan JM, Lee K, Smolka MB and Haber JE (2019) Mec1(ATR)
845 autophosphorylation and Ddc2(ATRIP) phosphorylation regulates dna damage checkpoint signaling *Cell*
846 *Rep* 28: 1090-1102 e1093

847 Menin L, Ursich S, Trovesi C, Zellweger R, Lopes M, Longhese MP and Clerici M (2018) Tel1/ATM
848 prevents degradation of replication forks that reverse after Topoisomerase poisoning *EMBO Rep* 19:
849 e45535

850 Moldovan GL, Pfander B and Jentsch S (2007) PCNA, the maestro of the replication fork *Cell* 129: 665-
851 679

852 Niu H and Klein HL (2017) Multifunctional roles of *Saccharomyces cerevisiae* Srs2 protein in replication,
853 recombination and repair *FEMS Yeast Res* 17: fow111

854 Ohouo PY, Bastos de Oliveira FM, Almeida BS and Smolka MB (2010) DNA damage signaling recruits
855 the Rtt107-Slx4 scaffolds via Dpb11 to mediate replication stress response *Mol Cell* 39: 300-306

856 Ohouo PY, Bastos de Oliveira FM, Liu Y, Ma CJ and Smolka MB (2013) DNA-repair scaffolds dampen
857 checkpoint signalling by counteracting the adaptor Rad9 *Nature* 493: 120-124

858 Paciotti V, Clerici M, Lucchini G and Longhese MP (2000) The checkpoint protein Ddc2, functionally
859 related to *S. pombe* Rad26, interacts with Mec1 and is regulated by Mec1-dependent phosphorylation in
860 budding yeast *Genes Dev* 14: 2046-2059

861 Papouli E, Chen S, Davies AA, Huttner D, Krejci L, Sung P and Ulrich HD (2005) Crosstalk between
862 SUMO and ubiquitin on PCNA is mediated by recruitment of the helicase Srs2p *Mol Cell* 19: 123-133

863 Pellicioli A, Lee SE, Lucca C, Foiani M and Haber JE (2001) Regulation of *Saccharomyces* Rad53
864 checkpoint kinase during adaptation from DNA damage-induced G2/M arrest *Mol Cell* 7: 293-300

865 Pfander B, Moldovan GL, Sacher M, Hoege C and Jentsch S (2005) SUMO-modified PCNA recruits Srs2
866 to prevent recombination during S phase *Nature* 436: 428-433

867 Pommier Y, Nussenzweig A, Takeda S and Austin C (2022) Human topoisomerases and their roles in
868 genome stability and organization *Nat Rev Mol Cell Biol* 23: 407-427

869 Psakhye I and Jentsch S (2012) Protein group modification and synergy in the SUMO pathway as
870 exemplified in DNA repair *Cell* 151: 807-820

871 Redon C, Pilch DR, Rogakou EP, Orr AH, Lowndes NF and Bonner WM (2003) Yeast histone 2A serine
872 129 is essential for the efficient repair of checkpoint-blind DNA damage *EMBO Rep* 4: 678-684

873 Regan-Mochrie G, Hoggard T, Bhagwat N, Lynch G, Hunter N, Remus D, Fox CA and Zhao X (2022)
874 Yeast ORC sumoylation status fine-tunes origin licensing *Genes Dev* 36: 807-821

875 Sanchez Y, Bachant J, Wang H, Hu F, Liu D, Tetzlaff M and Elledge SJ (1999) Control of the DNA
876 damage checkpoint by Chk1 and Rad53 protein kinases through distinct mechanisms *Science* 286: 1166-
877 1171

878 Saponaro M, Callahan D, Zheng X, Krejci L, Haber JE, Klein HL and Liberi G (2010) Cdk1 targets Srs2 to
879 complete synthesis-dependent strand annealing and to promote recombinational repair *PLoS Genet* 6:
880 e1000858

881 Seeber A *et al* (2016) RPA Mediates Recruitment of MRX to Forks and Double-Strand Breaks to Hold
882 Sister Chromatids Together *Mol Cell* 64: 951-966

883 Shorrocks AK, Jones SE, Tsukada K, Morrow CA, Belblidia Z, Shen J, Vendrell I, Fischer R, Kessler BM
884 and Blackford AN (2021) The Bloom syndrome complex senses RPA-coated single-stranded DNA to
885 restart stalled replication forks *Nat Commun* 12: 585

886 Smith J and Rothstein R (1995) A mutation in the gene encoding the Saccharomyces cerevisiae single-
887 stranded DNA-binding protein Rfa1 stimulates a RAD52-independent pathway for direct-repeat
888 recombination *Mol Cell Biol* 15: 1632-1641

889 Sogo JM, Lopes M and Foiani M (2002) Fork reversal and ssDNA accumulation at stalled replication forks
890 owing to checkpoint defects *Science* 297: 599-602

891 Sun Y, Saha S, Wang W, Saha LK, Huang SN and Pommier Y (2020) Excision repair of topoisomerase
892 DNA-protein crosslinks (TOP-DPC) *DNA Repair (Amst)* 89: 102837

893 Tercero JA, Longhese MP and Diffley JFX (2003) A central role for DNA replication forks in checkpoint
894 activation and response *Mol Cell* 11: 1323-1336

895 Ulrich HD and Davies AA (2009) In vivo detection and characterization of sumoylation targets in
896 *Saccharomyces cerevisiae Methods Mol Biol* 497: 81-103

897 Umezu K, Sugawara N, Chen C, Haber JE and Kolodner RD (1998) Genetic analysis of yeast RPA1
898 reveals its multiple functions in DNA metabolism *Genetics* 148: 989-1005

899 Usui T, Foster SS and Petrini JH (2009) Maintenance of the DNA-damage checkpoint requires DNA-
900 damage-induced mediator protein oligomerization *Mol Cell* 33: 147-159

901 Usui T, Ogawa H and Petrini JH (2001) A DNA damage response pathway controlled by Tel1 and the
902 Mre11 complex *Mol Cell* 7: 1255-1266

903 Wan B, Wu J, Meng X, Lei M and Zhao X (2019) Molecular Basis for Control of Diverse Genome Stability
904 Factors by the Multi-BRCT Scaffold Rtt107 *Mol Cell* 75: 238-251 e235

905 Wang H, Liu D, Wang Y, Qin J and Elledge SJ (2001) Pds1 phosphorylation in response to DNA damage
906 is essential for its DNA damage checkpoint function *Genes Dev* 15: 1361-1372

907 Waterman DP, Haber JE and Smolka MB (2020) Checkpoint responses to DNA double-strand breaks
908 *Annu Rev Biochem* 89: 103-133

909 Zhao X and Blobel G (2005) A SUMO ligase is part of a nuclear multiprotein complex that affects DNA
910 repair and chromosomal organization *Proc Natl Acad Sci U S A* 102: 4777-4782

911 Zhao X, Muller EG and Rothstein R (1998) A suppressor of two essential checkpoint genes identifies a
912 novel protein that negatively affects dNTP pools *Mol Cell* 2: 329-340

913 Zhao X and Rothstein R (2002) The Dun1 checkpoint kinase phosphorylates and regulates the
914 ribonucleotide reductase inhibitor Sml1 *Proc Natl Acad Sci U S A* 99: 3746-3751

915 Zou L and Elledge SJ (2003) Sensing DNA damage through ATRIP recognition of RPA-ssDNA
916 complexes *Science* 300: 1542-1548
917
918

Supplemental Materials

Figure S1. *srs2* mutants examined for CPT sensitivity and interactions with *rfa1* mutant.
(A) *srs2* mutants exhibit different levels of CPT sensitivity. *srs2-ΔPIM* showed slow growth on 8 µg/ml CPT. Sensitivity *srs2-SIM^{MUT}* toward CPT was seen at three CPT concentrations. *srs2-7AV* showed slow growth on media containing 4 and 8 µg/ml CPT. *srs2Δ* and *rfa1-zm2* are mutually suppressive for CPT sensitivity. Experiments are performed as in Figure 2C.
(B) *srs2-ΔPIM* confers better suppression of *rfa1-zm2's* CPT and MMS sensitivity than *srs2-3KR*. We note that mild suppression of *rfa1-zm2* by *srs2-3KR* was only seen at 0.03% MMS plates. Experiments are performed as in Figure 2C, and incubation times are noted. Dashed lines indicate the removal of superfluous rows.
(C) *srs2-ΔPIM* suppresses *rfa1-t33* sensitivity toward MMS. Dashed lines indicate the removal of superfluous rows.

Figure S2. *srs2-Δpim* cells exhibit increased levels of Rfa1 on chromatin.
(A) *rfa1-zm2* suppresses increased levels of Rfa1 in the chromatin fraction seen in *srs2-ΔPIM*. Rfa1 in chromatin and non-chromatin fractions as well as in total cell extracts was examined for strains with indicated genotypes. Histone H3 and Pgk1 were used as markers for chromatin and nonchromatin fractions, respectively.
(B) The relative levels of chromatin-bound Rfa1 after being normalized to H3 levels is shown. Mean of three biological isolates per genotype is graphed, with error bars representing standard deviation (SD). Statistical analysis was performed using pairwise Student's t-test. *, $p < 0.05$

Figure S3. Confirmation of Srs2 sumoylation and Mec1-S1964 phosphorylation.
(A) Detection of Srs2 sumoylation. Protein extracts from asynchronous cells were bound to Ni-NTA beads and the elutes were examined by immunoblotting using an anti-Srs2 antibody. Sumoylated Srs2 form was detected in wild-type cells expressing 8His-tagged SUMO (Smt3) but not in cells lacking this construct or in *srs2Δ* cells. Unmodified Srs2 showed unspecific Ni-NTA bead binding, thus being detectable in cells containing Srs2 regardless of the SUMO status.
(B) Detection of Mec1-S1964 phosphorylation. Cells were treated with CPT for 2 hours before immunoprecipitating Ddc2-myc was conducted. Ddc2 and the co-immunoprecipitated Mec1 were examined by immunoblotting. Phosphorylation of Ser1964 of the Mec1 protein was detected using the anti-Mec1-S1964-p antibody. This antibody also detected a non-specific band (*). Cells containing untagged Ddc2 or the *mec1-S1964A* mutation were used as controls.

Figure S4. Examination of Mec1-S964 phosphorylation.
(A) *mec1-S1964A* does not affect the CPT sensitivity of *srs2-3KR* or *srs2-3KR rfa1-zm2* cells. Experiments were performed as in Figure 2C.
(B) The effects of *mec1-S1964E* on the CPT sensitivity of *srs2-3KR* and *srs2-ΔPIM* cells with or without *rfa1-zm2*. Experiments were performed as in Figure 2C.
(C) *mec1-S1964A* or *-S1964E* does not affect Srs2 sumoylation. Experiments were performed as in Figure 4A. Mean values of three biological isolates per genotype are graphed, with error bars representing SD. Statistical analysis was performed using pairwise Student's t-test; no significance was found between values of wild-type and mutant strains.

Figure S5. *srs2-Y775A* improves *rfa1-zm2* mutant growth on CPT containing media.
The endogenous *SRS2* gene was deleted in cells, while the wild-type *SRS2* or the *srs2-Y775A* allele was integrated at the *HIS3* locus (Meir *et al.*, 2023). The control strain contains vector

969 sequence integrated at the *HIS3* locus (Meir *et al.*, 2023). Experiments were performed as in
970 Figure 2C.
971
972

973 **Table S1: Strains Sources.**
974
975 All strains are derived from W1588-4C, a *RAD5* derivative of W303 (*MATa ade2-1 can1-100*
976 *ura3-1 his3-11,15, leu2-3, 112 trp1-1 rad5-535*). Only one strain is listed per each genotype, but
977 at least two independent isolates of each genotype were used in the experiments.
978

Strain	Genotype	Source	Used In Figures
G16	Wild-type W303 *RAD5* strain	Lab collection	1B, 2C-E, 3B-C, 5C, 6B-D, S1-5
X8047-14B	*srs2Δ*	(Dhingra *et al.*, 2021)	6C-D, S1A, S3A
X8665-12-22D	*MATa srs2-ΔPIM*	This study	1B, 2C, 3B-C, 6B, S1A-C, S2
X8198-15B	*srs2-SIM^{MUT}*	This study	1B, 2D, S1A
G1114	*MATa srs2-7AV::HIS3*	(Saponaro *et al.*, 2010)	1B, 2D, S1A
X8650-2-1D	*MATa srs2-3KR::NAT*	This study	1B, 2C, 3B-C, S1A-C
X8659-14A	*MATa srs2-2SA*	This study	1B, 2D, S1A
G854	*MATα srs2-Δ(875-902)::HPH*	(Colavito *et al.*, 2009)	1B, 2D, S1A
X8047-1B	*MATα rfa1-zm2*	(Dhingra *et al.*, 2021)	2C, 2C-D, 3B-C, 6B, S1A-B, S2, S4B
X8650-2C	*MATa srs2-3KR::NAT rfa1-zm2*	This study	2C, 3B-C, S1B, S4A-B
X8666-35-6A	*MATa srs2-ΔPIM rfa1-zm2*	This study	2C, 3B-C, 6B, S1B, S2, S4B
X8210-2B	*MATa rfa1-t33*	(Dhingra *et al.*, 2021)	2E, S1C
X8745-2A	*MATa srs2-3KR::NAT rfa1-t33*	This study	2E, S1C
X8743-13A	*MATα srs2-ΔPIM rfa1-t33*	This study	2E, S1C
X8198-15A	*srs2-SIM^{MUT} rfa1-zm2*	This study	2D
X8637-6B	*MATa srs2-7AV::HIS3 rfa1-zm2*	This study	2D
X8137-10B	*MATa srs2-Δ875-902::HPH rfa1-zm2*	This study	2D
X8660-4B	*MATα srs2-2SA rfa1-zm2*	This study	2D
T1358-2	*MATa 8His-SMT3::TRP1*	Lab Collection	5A-B, 5E
X8898-19D	*MATa srs2-Δ::HIS3 8His-SMT3::TRP1*	This study	S3A
X8808-2D	*MATa srs2-ΔPIM 8His-SMT3::TRP1*	This study	5A
X8795-9D	*MATa srs2-3KR::NAT 8His-SMT3::TRP1*	This study	5A
X8807-6A	*MATa sml1Δ::URA3 8His-SMT3::TRP1*	This study	5E
X8746-4D	*MATa sml1Δ::URA3 mec1Δ::TRP1 8His-SMT3::TRP1*	This study	5E
X8807-7A	*MATa sml1Δ::URA3 rad53Δ::HIS3 8His-SMT3::TRP1*	This study	5E
X9055-1D	*MATa DDC2-Myc18::HIS3*	This study	6A, S3B
X9190-8A	*MATa DDC2-Myc18::HIS3 mec1-S1964A*	This study	S3B
X9225-3A	*MATa mec1-S1964A*	This study	6B
X9225-3C	*MATa mec1-S1964A rfa1-zm2*	This study	6B
X9088-38C	*MATa mec1-S1964A srs2-ΔPIM*	This study	6B
X9225-1B	*MATα mec1-S1964A srs2-ΔPIM rfa1-zm2*	This study	6B
X8495-5D	*MATa rfa1-S178D*	This study	6C
X8495-2D	*MATa srs2Δ::HIS3 rfa1-S178D*	This study	6C
X8494-3B	*MATa rfa1-S178A*	This study	6C

X8494-3A	*MATa srs2Δ::HIS3 rfa1-S178A*	This study	6C
X8658-14-22D	*MATa rfa2-3SA*	This study	6D
X8658-14-13C	*MATa srs2Δ::HIS3 rfa2-3SA*	This study	6D
X8779-13D	*MATa rfa2-3SD*	This study	6D
X8779-13B	*MATa srs2Δ rfa2-3SD*	This study	6D
X9265-4D	*MATa SLX4-TAP::HIS3*	(Wan *et al.*, 2019)	4A-C
X9265-4A	*MATa srs2-ΔPIM SLX4-TAP::HIS3*	This study	4A-C
X8956-7C	*MATa slx4^{RIM}-TAP::HIS3*	(Wan *et al.*, 2019)	4A-C
X8956-5D	*MATa srs2-ΔPIM slx4^{RIM}-TAP::HIS3*	This study	4A-C
X9228-2D	*MATa mec1-S1964A srs2-3KR::NAT*	This study	S4A
X9228-5A	*MATα mec1-S1964A srs2-3KR::NAT rfa1-zm2*	This study	S4A
X9090-9C	*MATa mec1-S1964E*	This study	S4B
X9091-14A	*MATa mec1-S1964E rfa1-zm2*	This study	S4B
X9090-19A	*MATa mec1-S1964E srs2-ΔPIM*	This study	S4B
X9132-15B	*MATa mec1-S1964E srs2-ΔPIM rfa1-zm2*	This study	S4B
X9091-13A	*MATa mec1-S1964E srs2-3KR::NAT*	This study	S4B
X9132-10B	*MATα mec1-S1964E srs2-3KR::NAT rfa1-zm2*	This study	S4B
X9137-3B	*MATa mec1-S1964A 8His-SMT3::TRP1*	This study	S4C
X9136-2B	*MATa mec1-S1964E 8His-SMT3::TRP1*	This study	S4C
X9486-5B	*MATa his3::pRS303-p500-SRS2::HIS3 srs2Δ::KanMX*	This study	S5
X9485-8D	*MATa his3::pRS303-p500::HIS3 srs2Δ::KanMX*	This study	S5
X9485-8B	*MATa rfa1-zm2 his3::pRS303-p500::HIS3 srs2Δ::KanMX*	This study	S5
X9486-1D	*MATa rfa1-zm2 his3::pRS303-p500-SRS2::HIS3 srs2Δ::KanMX*	This study	S5
X9484-9C	*MATa rfa1-zm2 his3::pRS303-p500-Srs2-Y775A::HIS3 srs2Δ::KanMX*	This study	S5
X9484-18D	*MATa his3::pRS303-p500-Srs2-Y775A::HIS3 srs2Δ::KanMX*	This study	S5

979

Fig. 1

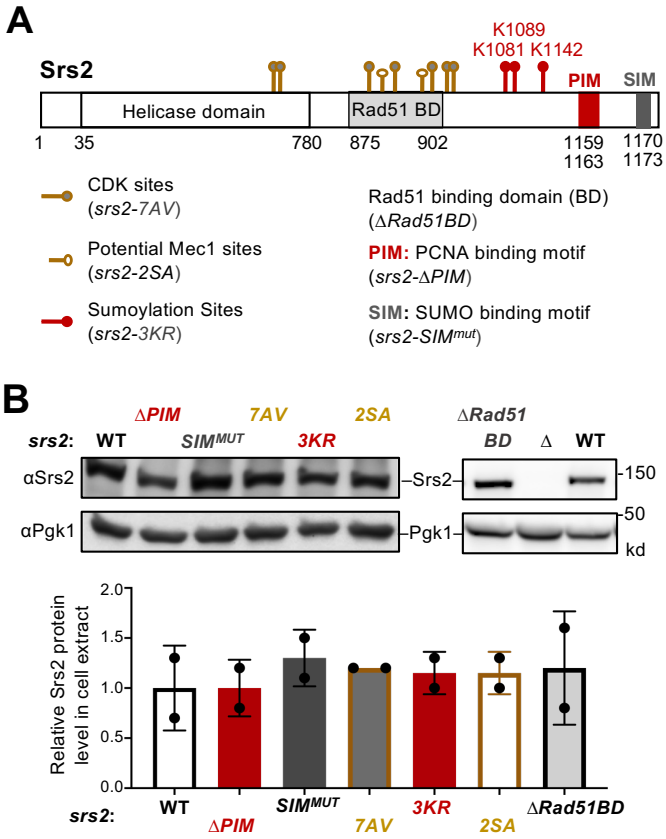
A
Srs2
K1089
K1081 K1142
PIM
SIM
Helicase domain
Rad51 BD
1
35
780
875
902
1159
1163
1170
1173
CDK sites
(srs2-7AV)
Potential Mec1 sites
(srs2-2SA)
Sumoylation Sites
(srs2-3KR)
Rad51 binding domain (BD)
(ΔRad51BD)
PIM: PCNA binding motif
(srs2-ΔPIM)
SIM: SUMO binding motif
(srs2-SIMmut)
B
ΔPIM
7AV
2SA
ΔRad51
srs2:
WT
SIMMUT
3KR
BD
Δ
WT
αSrs2
αPgk1
Srs2
Pgk1
150
50
kd
Relative Srs2 protein level in cell extract
2.0
1.5
1.0
0.5
0.0
srs2:
WT
ΔPIM
SIMMUT
7AV
3KR
2SA
ΔRad51BD

Fig. 2

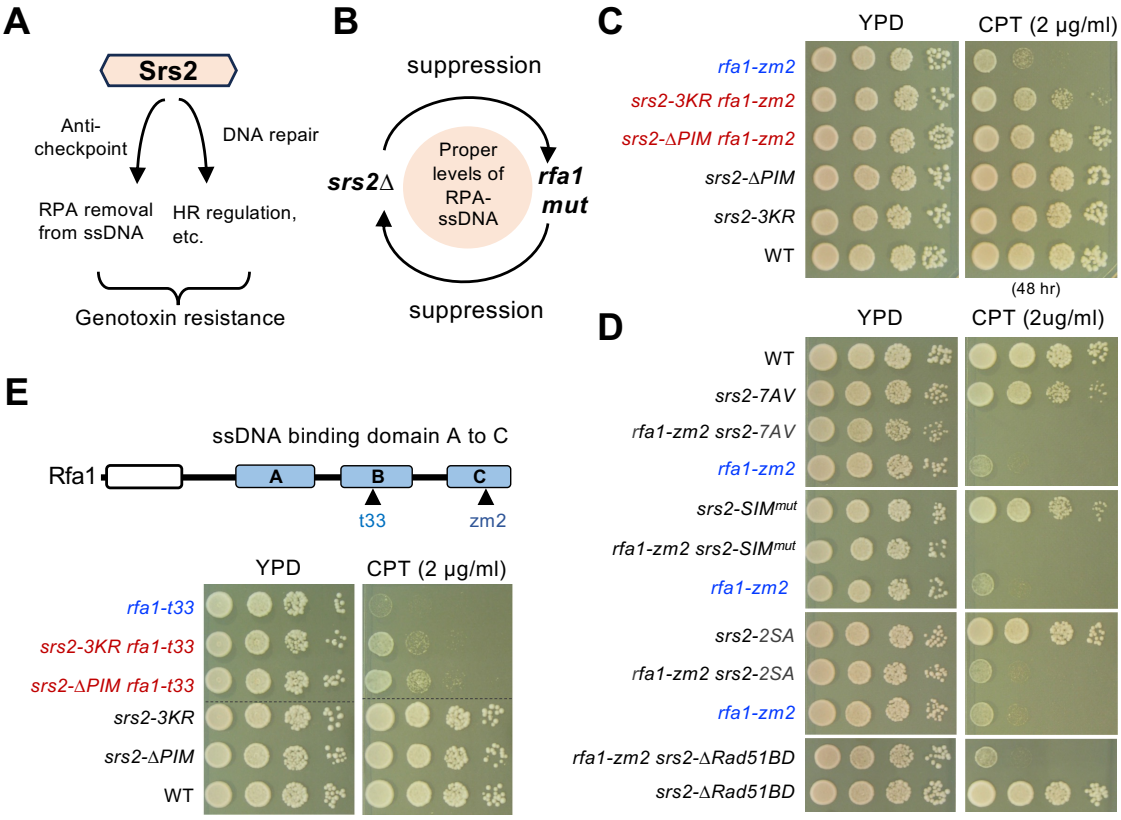
A
Srs2
Anti-checkpoint
DNA repair
RPA removal from ssDNA
HR regulation, etc.
Genotoxin resistance
B
suppression
srs2Δ
Proper levels of RPA-ssDNA
rfa1 mut
suppression
C
YPD
CPT (2 μg/ml)
rfa1-zm2
srs2-3KR rfa1-zm2
srs2-ΔPIM rfa1-zm2
srs2-ΔPIM
srs2-3KR
WT
(48 hr)
D
YPD
CPT (2ug/ml)
WT
srs2-7AV
rfa1-zm2 srs2-7AV
rfa1-zm2
srs2-SIMmut
rfa1-zm2 srs2-SIMmut
rfa1-zm2
srs2-2SA
rfa1-zm2 srs2-2SA
rfa1-zm2
rfa1-zm2 srs2-ΔRad51BD
srs2-ΔRad51BD
E
ssDNA binding domain A to C
Rfa1
A
B
C
t33
zm2
YPD
CPT (2 μg/ml)
rfa1-t33
srs2-3KR rfa1-t33
srs2-ΔPIM rfa1-t33
srs2-3KR
srs2-ΔPIM
WT

Fig. 3

A

Mutants	Checkpoint levels	Interpretations
rfa1-zm2	Increased	Suboptimal RPA levels on DNA lead to increased DNA lesions and checkpoint activation
rfa1-zm2 *srs2Δ (srs2-ΔPIM or srs2-3KR)*	Normal	RPA levels on DNA and checkpoint levels are restored compared with *rfa1-zm2*
srs2-ΔPIM or srs2-3KR	Normal	Mild-defects of partially defective *srs2* alleles is masked by other checkpoint dampening proteins

B

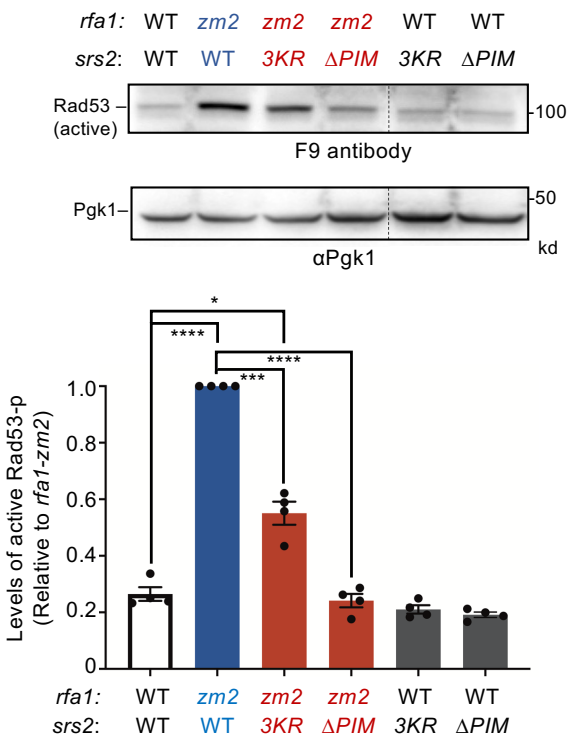

C

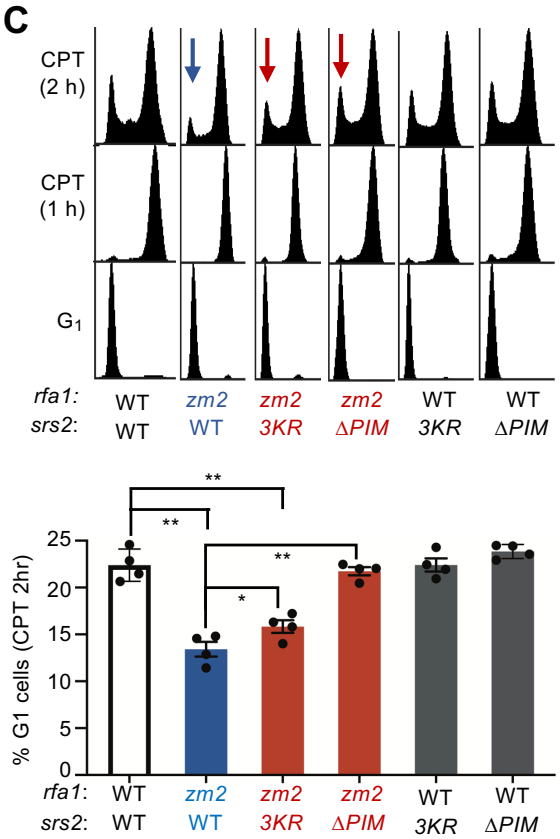

Fig. 4

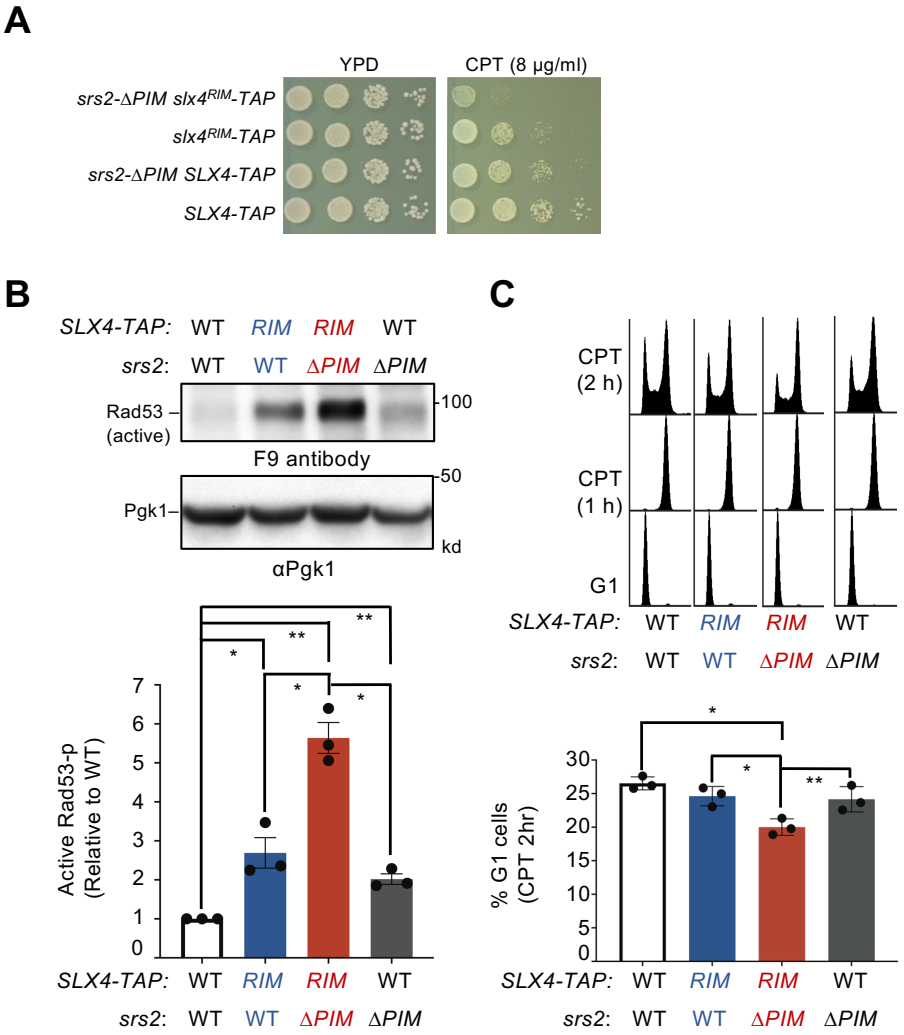
A
YPD
CPT (8 μg/ml)
srs2-ΔPIM slx4RIM-TAP
slx4RIM-TAP
srs2-ΔPIM SLX4-TAP
SLX4-TAP
B
SLX4-TAP: WT RIM RIM WT
srs2: WT WT ΔPIM ΔPIM
Rad53 (active)
100
F9 antibody
50
Pgk1
kd
αPgk1
Active Rad53-p (Relative to WT)
0
1
2
3
4
5
6
7
*
**
**
*
*
SLX4-TAP: WT RIM RIM WT
srs2: WT WT ΔPIM ΔPIM
C
CPT (2 h)
CPT (1 h)
G1
SLX4-TAP: WT RIM RIM WT
srs2: WT WT ΔPIM ΔPIM
% G1 cells (CPT 2hr)
0
5
10
15
20
25
30
*
*
**
SLX4-TAP: WT RIM RIM WT
srs2: WT WT ΔPIM ΔPIM

Fig. 5

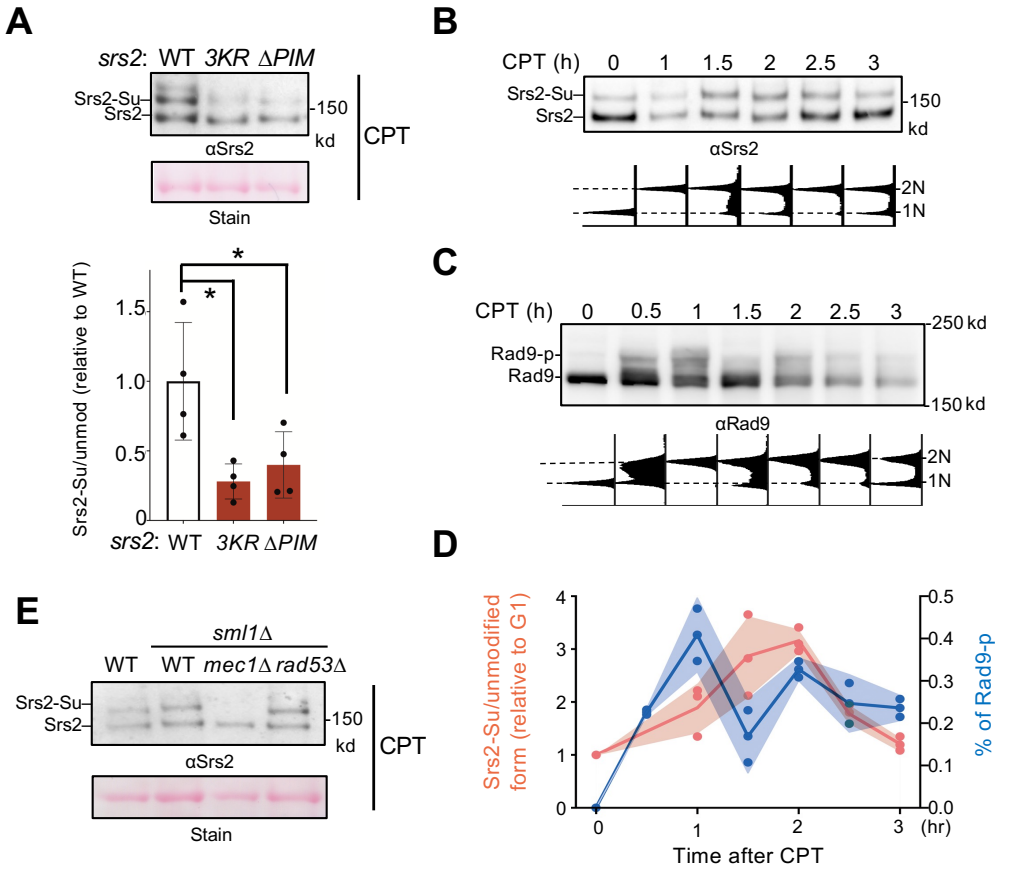
A
srs2: WT 3KR ΔPIM
Srs2-Su
Srs2
150 kd
αSrs2
CPT
Stain
Srs2-Su/unmod (relative to WT)
1.5
1.0
0.5
0
srs2: WT 3KR ΔPIM
B
CPT (h) 0 1 1.5 2 2.5 3
Srs2-Su
Srs2
150 kd
αSrs2
2N
1N
C
CPT (h) 0 0.5 1 1.5 2 2.5 3
250 kd
Rad9-p
Rad9
150 kd
αRad9
2N
1N
D
Srs2-Su/unmodified form (relative to G1)
% of Rad9-p
Time after CPT
(hr)
E
sml1Δ
WT WT mec1Δ rad53Δ
Srs2-Su
Srs2
150 kd
αSrs2
CPT
Stain

Fig. 6

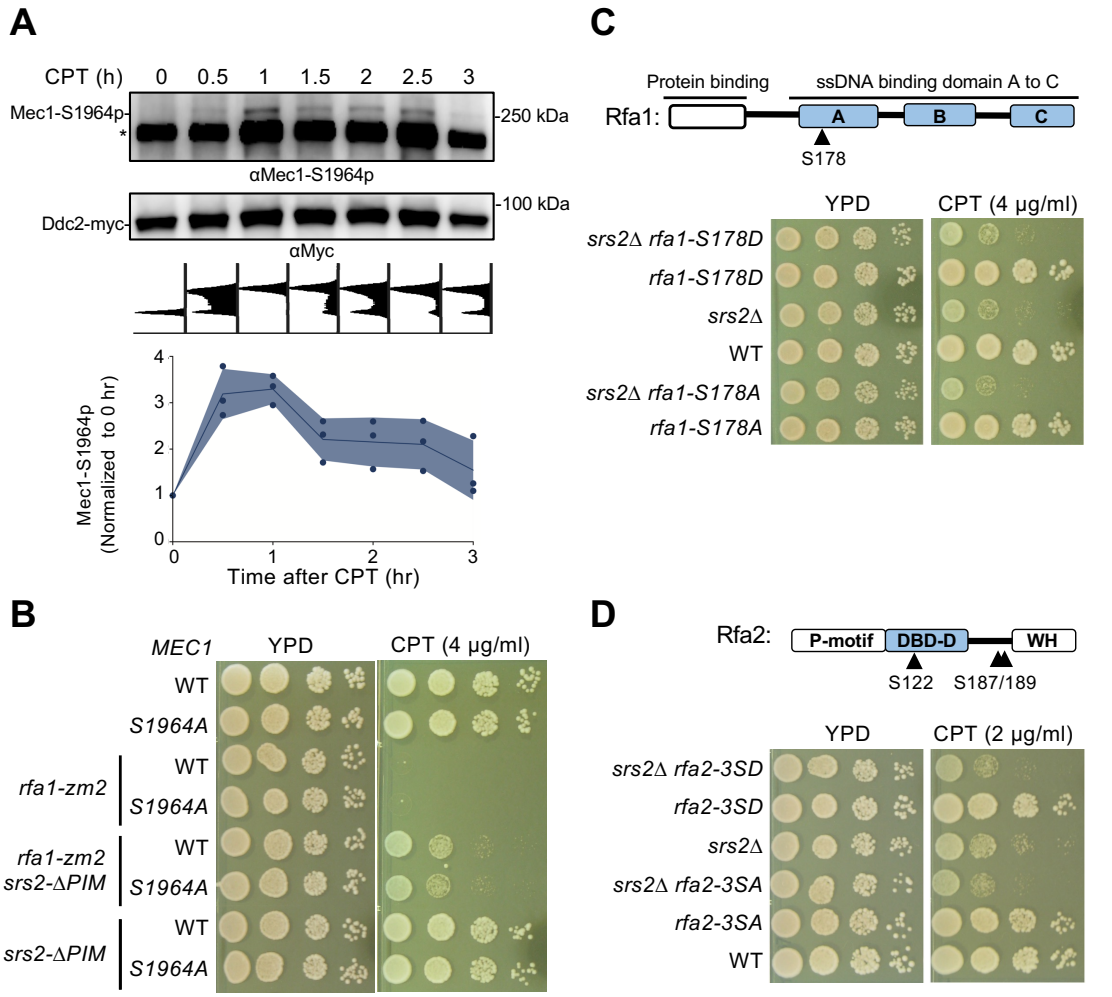
A
CPT (h) 0 0.5 1 1.5 2 2.5 3
Mec1-S1964p
*
250 kDa
αMec1-S1964p
Ddc2-myc
100 kDa
αMyc
Mec1-S1964p (Normalized to 0 hr)
Time after CPT (hr)
B
MEC1
YPD
CPT (4 μg/ml)
WT
S1964A
rfa1-zm2
rfa1-zm2 srs2-ΔPIM
srs2-ΔPIM
C
Protein binding
ssDNA binding domain A to C
Rfa1:
A
B
C
S178
srs2Δ rfa1-S178D
rfa1-S178D
srs2Δ
WT
srs2Δ rfa1-S178A
rfa1-S178A
D
Rfa2:
P-motif
DBD-D
WH
S122
S187/189
CPT (2 μg/ml)
srs2Δ rfa2-3SD
rfa2-3SD
srs2Δ
srs2Δ rfa2-3SA
rfa2-3SA
WT

Fig. 7

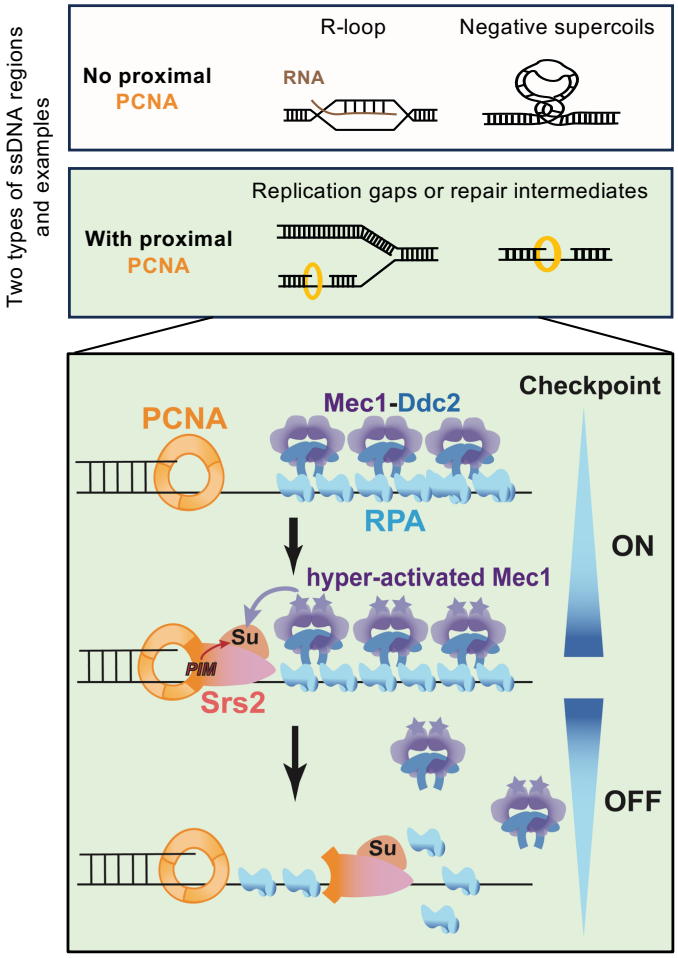
Two types of ssDNA regions and examples
No proximal PCNA
R-loop
RNA
Negative supercoils
With proximal PCNA
Replication gaps or repair intermediates
Checkpoint
PCNA
Mec1-Ddc2
RPA
ON
hyper-activated Mec1
Su
PIM
Srs2
OFF
Su

Fig. S1

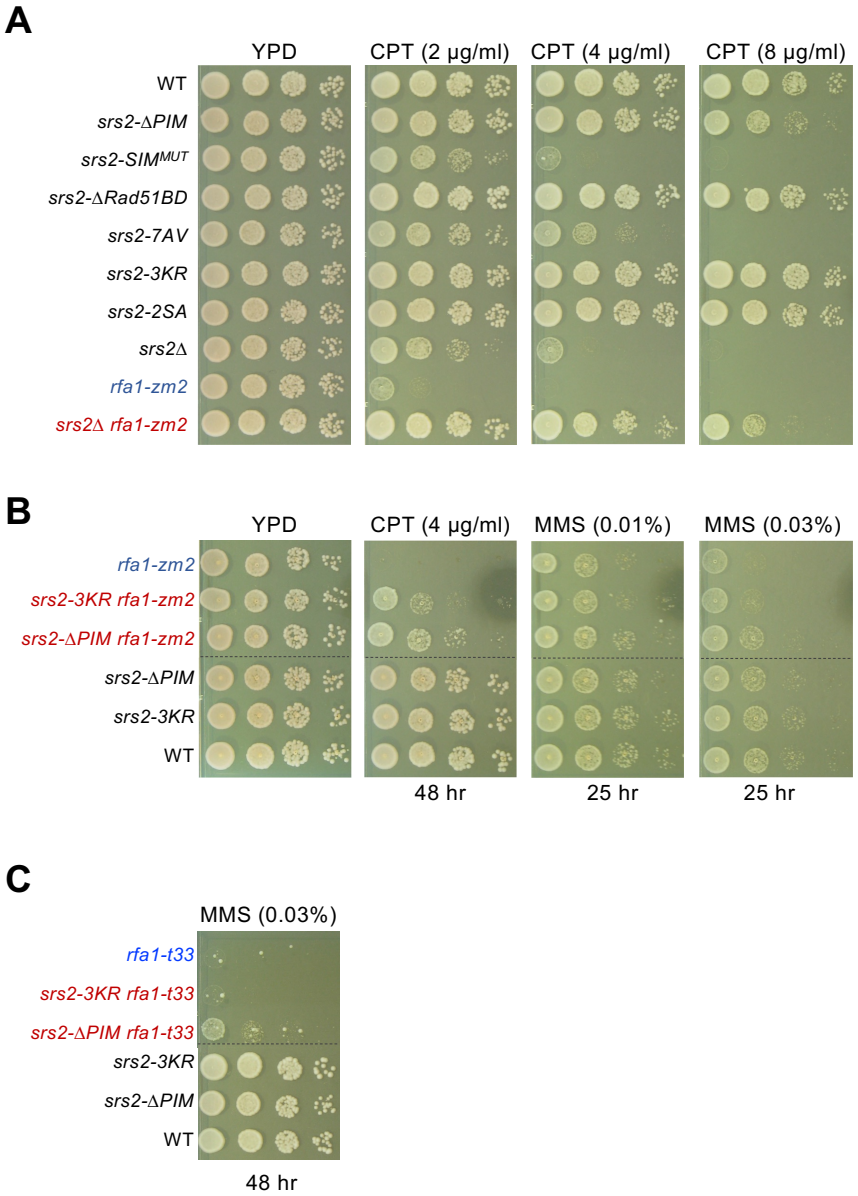
A
YPD
CPT (2 μg/ml)
CPT (4 μg/ml)
CPT (8 μg/ml)
WT
srs2-ΔPIM
srs2-SIM^MUT
srs2-ΔRad51BD
srs2-7AV
srs2-3KR
srs2-2SA
srs2Δ
rfa1-zm2
srs2Δ rfa1-zm2
B
YPD
CPT (4 μg/ml)
MMS (0.01%)
MMS (0.03%)
rfa1-zm2
srs2-3KR rfa1-zm2
srs2-ΔPIM rfa1-zm2
srs2-ΔPIM
srs2-3KR
WT
48 hr
25 hr
25 hr
C
MMS (0.03%)
rfa1-t33
srs2-3KR rfa1-t33
srs2-ΔPIM rfa1-t33
srs2-3KR
srs2-ΔPIM
WT
48 hr

Fig. S2

A

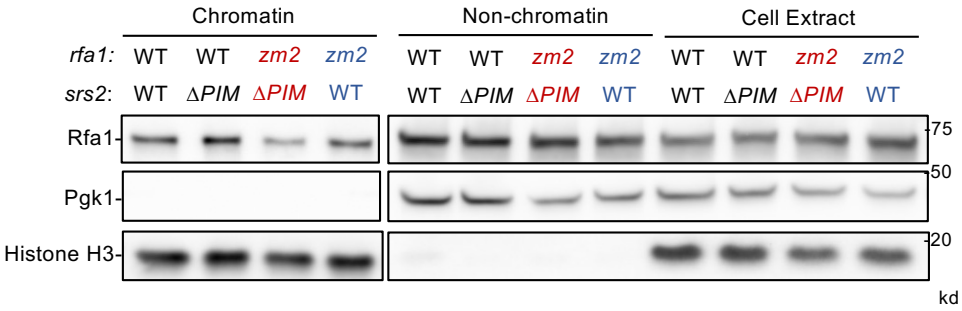
Chromatin
Non-chromatin
Cell Extract
rfa1: WT WT zm2 zm2 WT WT zm2 zm2 WT WT zm2 zm2
srs2: WT ΔPIM ΔPIM WT WT ΔPIM ΔPIM WT WT ΔPIM ΔPIM WT
Rfa1
Pgk1
Histone H3
75
50
20
kd

B

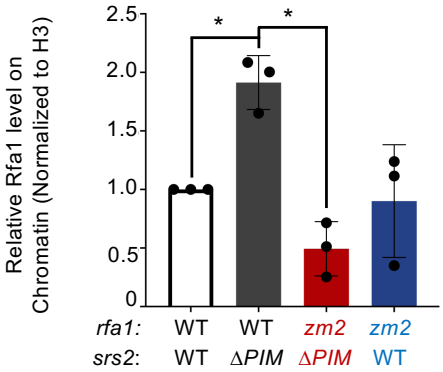
Relative Rfa1 level on Chromatin (Normalized to H3)
2.5
2.0
1.5
1.0
0.5
0
*
*
rfa1: WT WT zm2 zm2
srs2: WT ΔPIM ΔPIM WT

Fig. S3

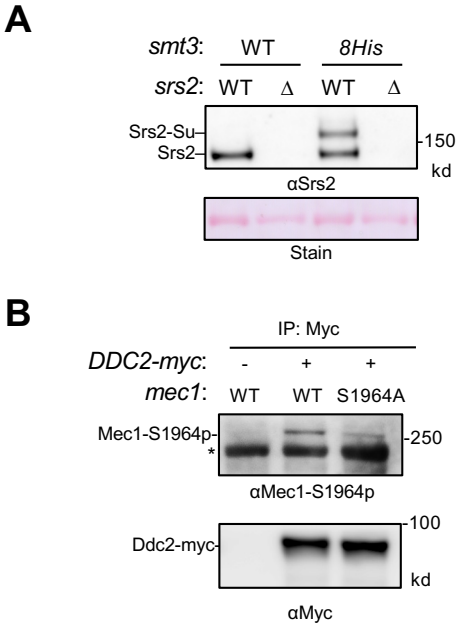
A
smt3: WT 8His
srs2: WT Δ WT Δ
Srs2-Su
Srs2
150
kd
αSrs2
Stain
B
IP: Myc
DDC2-myc: - + +
mec1: WT WT S1964A
Mec1-S1964p
*
250
αMec1-S1964p
100
Ddc2-myc
kd
αMyc

Fig. S4

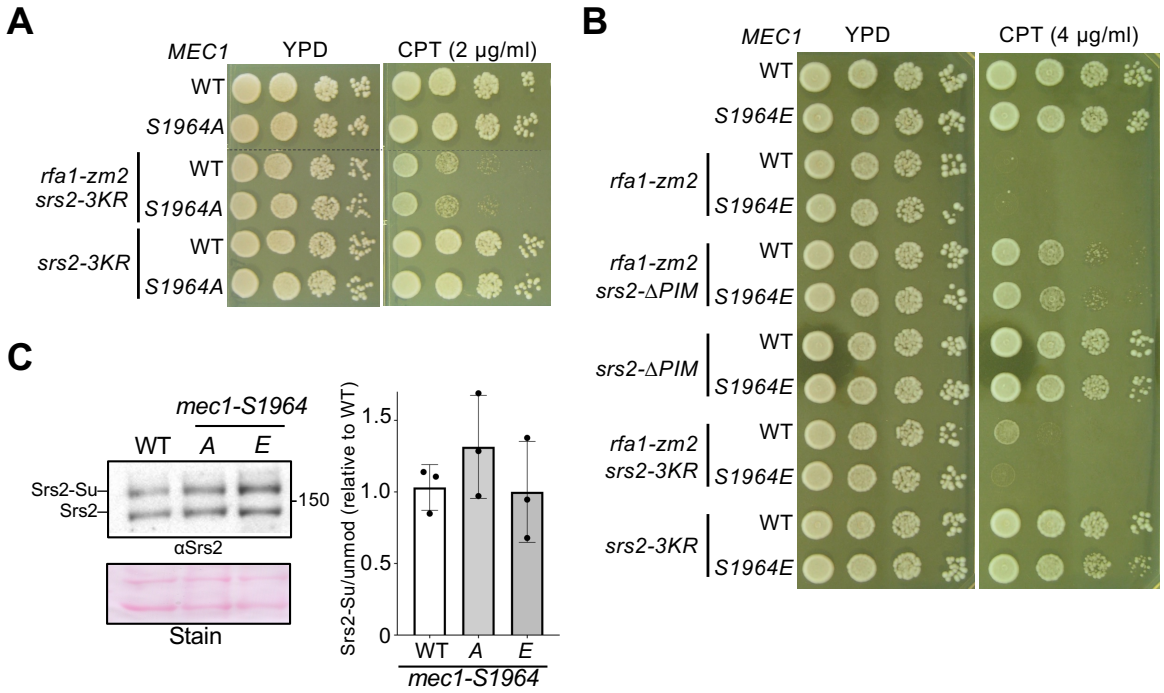
A
MEC1
YPD
CPT (2 μg/ml)
WT
S1964A
rfa1-zm2
srs2-3KR
WT
S1964A
srs2-3KR
WT
S1964A
B
MEC1
YPD
CPT (4 μg/ml)
WT
S1964E
rfa1-zm2
WT
S1964E
rfa1-zm2
srs2-ΔPIM
WT
S1964E
srs2-ΔPIM
WT
S1964E
rfa1-zm2
srs2-3KR
WT
S1964E
srs2-3KR
WT
S1964E
C
mec1-S1964
WT
A
E
Srs2-Su
Srs2
150
αSrs2
Stain
Srs2-Su/unmod (relative to WT)
1.5
1.0
0.5
0
WT
A
E
mec1-S1964

Fig. S5

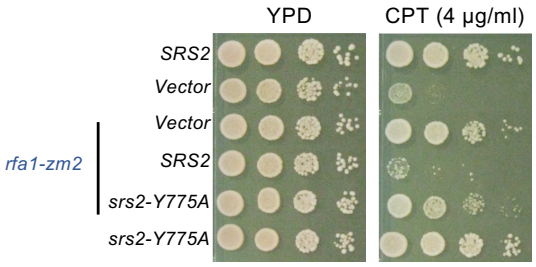

Endogenous *SRS2* deleted in all cells.